How subsurface and double-core anticyclones intensify the winter mixed layer deepening in the Mediterranean sea

Alexandre Barboni[1,2], Solange Coadou-Chaventon[3], Alexandre Stegner[1], Briac Le Vu[1], and Franck Dumas[2,4]

[1]Laboratoire de Météorologie Dynamique, IPSL, Ecole Polytechnique, 91128 Palaiseau, France
[2]Département de Recherche en Océanographie Physique, Service Hydrographique et Océanographique de la Marine (SHOM), 13, rue du Chatellier 29200 Brest, France
[3]Département de Géosciences, Ecole normale supérieure, 24 rue Lhomond, 75005 Paris, France
[4]Laboratoire d'Océanographie Physique et Spatiale, Equipe côtière, rue Dumont Durville, 29280 Plouzané

Correspondence: Alexandre Barboni (alexandre.barboni@lmd.ipsl.fr), Solange Coadou-Chaventon (solange.coadou-chaventon@lmd.ipsl.fr)

Abstract. The mixed layer is the uppermost layer of the ocean, connecting the atmosphere to the subsurface ocean through atmospheric fluxes. It is subject to pronounced seasonal variations: it deepens in winter due to buoyancy loss and shallows in spring while heat flux increase and restratify the water column. A mixed layer depth (MLD) modulation over this seasonal cycle has been observed within mesoscale eddies. Taking advantage of the numerous Argo floats deployed and trapped within large Mediterranean anticyclones over the last decades, we reveal for the first time this modulation at a 10-day temporal scale and free of the smoothing effect of composite approaches. The analysis of 16 continuous MLD time series inside 13 long-lived anticyclones at a fine temporal scale brings to light the importance of the eddy preexisting vertical structure in setting the MLD modulation by mesoscale eddies. Extreme MLD anomalies of up to 330m are observed when the winter mixed layer connects with a preexisting subsurface anticyclonic core, greatly accelerating mixed layer deepening. The winter MLD sometimes does not achieve such connection but homogenizes another subsurface layer, then forming a multi-core anticyclone with spring restratification. A MLD restratification delay is always observed, reaching more than 2 months in 3 out the 16 MLD timeseries. The water column starts to restratify outside anticyclones while mixed layer keeps deepening and cooling at the eddy core for a longer time. These new elements provide new keys for understanding anticyclone vertical structure formation and evolution.

1 Introduction

The mixed layer corresponds to the ocean surface layer over which water properties are kept uniform through active mixing. It connects the atmosphere to the subsurface ocean through air-sea fluxes of heat, freshwater or other chemical components such as carbon (Takahashi et al., 2009; Large and Yeager, 2012). The mixed layer depth (MLD) controls how deep the mixing is acting, bringing water properties from below to the surface and the other way around. This depth is subject to pronounced seasonal variations, the mixed layer deepening with winter heat loss, while spring surface heating restratifies the column and the mixed layer gets shallower. Due to its importance for both ocean physics and biogeochemistry, global MLD climatologies were computed (de Boyer Montégut et al., 2004; Holte et al., 2017). Several MLD climatologies were also computed for the

Mediterranean sea (d'Ortenzio et al., 2005; Houpert et al., 2015), showing specific dynamics in winter convective regions such as the Gulf of Lion, the Egean and the Adriatic seas or the Rhodes gyre, with biological impacts on plankton bloom (d'Ortenzio and Ribera d'Alcalà, 2009; Lavigne et al., 2013). However large spread in MLD was also observed in regions hosting intense anticyclones such as the Algerian, Ionian and Levantine basins (Houpert et al., 2015), highlighting the need to take into account the local impact of mesoscale eddies.

Recent development of automatic eddy tracking algorithms and eddy atlases (at global scale see for example Chelton et al. (2011), Pegliasco et al. (2022) and in the Mediterranean see Stegner et al. (2019)), combined with an increase of in-situ measurements thanks to the development of autonomous platforms (Le Traon, 2013), recently allowed to study the influence of mesoscale oceanic eddies on the MLD. It is now well known that anticyclonic (respectively cyclonic) eddies tend to deepen (shoal) the MLD (Dufois et al., 2016; Hausmann et al., 2017; Gaube et al., 2019). Eddies actually amplify the MLD seasonal cycle, the deepest MLD anomaly being reached during winter (Hausmann et al., 2017; Gaube et al., 2019). A first mechanism was proposed by Williams (1988), the eddy-modulation of the MLD being related to their induced Sea Surface Temperature anomaly (SSTA). Indeed as shown by Hausmann and Czaja (2012), anticyclonic (cyclonic) eddies are usually associated to positive (negative) SSTA, and this is at least true in winter in the Mediterranean sea (Moschos et al., 2022). It leads to stronger (weaker) heat loss during the winter and triggering enhanced (reduced) ocean convection and therefore deeper (shallower) MLD. In addition Hausmann et al. (2017) in the Southern Ocean and Gaube et al. (2019) for the global ocean found out that the eddy MLD anomaly, computed from eddy composites, scales with the eddy SSH amplitude. Gaube et al. (2019) proposed the same linear trend at the global scale $\pm 1m$ MLD anomaly for each $1cm$ SSH for both cyclones and anticyclones. Physical drivers controlling the eddy-induced MLD are supported by other studies showing an eddy-modulation of air-sea exchanges. Villas Bôas et al. (2015) found ocean heat loss enhanced (respectively reduced) in anticyclones (cyclones) in energetic regions of the South Atlantic ocean, once again scaling with eddy amplitude, for both sensible and latent heat flux. Frenger et al. (2013) showed enhanced rainfall and cloud cover above anticyclones in the Southern ocean as a consequence of enhanced turbulent heat fluxes, but suggested a scaling with the eddy SSTA. Such relation should remain coherent, as Hausmann and Czaja (2012) also found anticyclone warm (cyclone cold) eddy SSTA to scale with the eddy amplitude in the Gulf Stream region. Altogether, eddy MLD anomalies are expected to be easily inferred provided that background measurements outside eddies are available, a promising link for remote sensing application.

However all these studies were at a coarse monthly temporal resolution, whereas mixed layer is driven by air-ocean fluxes and thus is expected to react at timescale close to the inertial period (D'Asaro, 1985; Lévy et al., 2012). If several studies showed the MLD and upper ocean stratification to vary over timescales of a week at regional scales (Lacour et al. (2019) in the North Atlantic or d'Ortenzio et al. (2021) in the Rhodes gyre), no studies are yet available on the temporal evolution of eddy MLD anomaly. A second limit in previous studies is the use of composite datasets that smooth out the non-linearities induced by eddies. If the composite analysis can provide a first order trend, this is likely not sufficient to quantify accurately the various impacts of the wide diversity of individual eddies varying in size and intensity. A third but linked limit - explicitly

pointed out by Villas Bôas et al. (2015) and Hausmann et al. (2017) - is their focus on surface-intensified eddies with the most coherent surface signature. Indeed the relation between eddy SSTA and SSH amplitude strongly relies on the hypothesis of a surface-intensified structure and Assassi et al. (2016) showed that it should not be the case for subsurface anticyclones.

60 Subsurface eddies are mesoscale structure were the density anomaly (compared to the outside-eddy density profile) is overlaid by an anomaly of opposite sign. For instance a subsurface anticyclone has a lighter core at depth overlaid by a negative density anomaly near the surface. Following the thermal wind equation, depth of maximal geostrophic speed is below the surface. The isopycnals and isotherms doming above a subsurface anticyclone core could greatly impact the upper layer stratification, and subsequently the inside-eddy mixed layer dynamics. In the South China sea and still using the composite method, He et al.

65 (2018) found the anticyclones to be predominantly subsurface eddies.They also observed a linear trend between the subsurface temperature anomaly and SSH on an annual average, and an eddy-induced MLD anomaly but based on monthly climatology and did not find a relationship with MLD. A more detailed comparison with more observational data and especially better temporal resolution is then lacking.

70 The Mediterranean sea is an interesting region to study eddy influence on MLD. At first, due to repeated oceanographic campaigns the density of in-situ measurements is relatively high and in particular several campaigns specifically targeted long-lived mesoscale anticyclones in both Western and Eastern basins. Without aiming for exhaustiveness, one can in particular list: EGYPT (Poulain et al., 2006), BOUM (Moutin and Prieur, 2012), 'Eye of the Levantine' (Hayes et al., 2011), PROTEVS (Garreau et al., 2018) and PERLE (Ioannou et al., 2019). Additionally several Argo profiling floats were launched inside eddies

75 and remained trapped for a long time (Ioannou et al., 2020), altogether allowing in the Mediterranean sea to accurately follow particular eddies and go beyond the averaged composite vision. Moreover data from these programs were often only analyzed in the scope on the campaigns, and an eddy study with a larger statistical focus is still lacking. A second relevance for Mediter-ranean eddies is the variety of mesoscale structures in terms of dynamics, from intense Algerian and Ierapetra anticyclones needing cyclogeostrophic corrections (Ioannou et al., 2019) to subsurface eddy with strong density anomalies but weak SSH

80 signature (Hayes et al., 2011). Moutin and Prieur (2012) also showed the vertical structure, in temperature and salinity, of mesoscale eddies to be very different from one basin to another. Barboni et al. (2021) showed the marked subsurface difference between a new anticyclone detached from the coast compared to an offshore structure having been tracked more than a year. All these structures should provide different examples of eddy-MLD interactions.

85 In the Mediterranean sea there is in addition a strong asymmetry between cyclones and anticyclones, remarkable in lifetime difference (Mkhinini et al., 2014). The deformation radius in the Mediterranean sea is indeed about 8 to 12 km (Kurkin et al., 2020), and cyclones are less stable when greater than the deformation radius and more subject to external shear (Arai and Ya-magata, 1994; Graves et al., 2006). This leads to cyclones being predominantly below the effective resolution of SSH products about 20km (Stegner et al., 2021). As a consequence anticyclones are coherent larger vortices, while cyclones in the Mediter-

90 ranean sea as detected by altimetry are instead cyclonic gyres bounded by topography or hydrographic fronts such as the Ligurian, South-Western Crete or Rhodes gyre (Stegner et al., 2021). MLD evolution inside these cyclonic gyres was already

surveyed because of their importance for biological production, in particular with the development of BGC-Argo (d'Ortenzio et al., 2021; Taillandier et al., 2022). Apart for specific campaigns, Mediterranean anticyclones remain poorly analyzed despite being more coherent, and statistical comparison based on vertical profiles is lacking, with the noticeable exception of the BOUM campaign surveying 3 anticyclones across the Mediterranean in 2008 (Moutin and Prieur, 2012).

This paper aims to study the temporal evolution of the mixed layer inside a wide diversity of long-lived anticyclones in the Mediterranean sea compared to the evolution of the background MLD. The goal is to quantify more precisely the local impacts of individual eddies on the winter mixed layer deepening. The paper is organized as follows. Section 2 describes the eddy detection and tracking algorithm and the in-situ profiles database. Section 3 details the methodology used to compute the MLD, colocalize profiles and eddies in order to quantify accurately the MLD anomalies induced by individual eddies. In the section 4 we analyze the MLD evolution at anticyclone cores, provide statistical analysis over the variety of structures surveyed and discuss the impact of complex vertical eddy structure on winter mixed layer deepening. Finally in the last section 5 we discuss the possible physical drivers and implication for these MLD anomalies.

2   Data

2.1   Anticyclone detections : the DYNED Atlas

Eddy detections are provided through the Angular Momentum Eddy Detection and Tracking Algorithm (AMEDA). AMEDA is a mixed velocity-altimetry approach, its relies on using primarily streamlines from a velocity field and identifying possible eddy centers computed as maxima of local normalized angular momentum (Le Vu et al., 2018). It was successfully used in several regions of the world ocean in altimetric data (Aroucha et al., 2020; Ayouche et al., 2021; Barboni et al., 2021), high frequency radar data (Liu et al., 2020) or numerical simulations (de Marez et al., 2021). From 1 January 2000 to 31 December 2019, AMEDA is applied on AVISO sea surface height (SSH) delayed-time product at a resolution of 1/8°with daily output. From 1 January 2020 to 31 December 2021, AMEDA is applied on AVISO SSH near-real-time day+6 product (Pujol, 2021), at the same spatial and temporal resolution. In each eddy single observation (one eddy observed one day), AMEDA gives a center and two contours. The 'maximal speed' contour is the enclosed streamline with maximal speed (i.e. in the geostrophic approximation, with maximal SSH gradient) ; it is assumed to be the limit of the eddy core region where water parcels are trapped. The 'end' contour is the outermost closed SSH contour surrounding the eddy center and the maximal speed contour ; it is assumed to be the area of the eddy footprint, larger than just its core but still influenced by the eddy shear (Le Vu et al., 2018). AMEDA gathers eddy observations in eddy tracks, allowing to follow the same structure in time and space, sometimes over several months. The eddy tracks collection in the whole Mediterranean sea constitutes the DYNED Atlas database (Stegner et al., 2019), and is available online (for the years 2000 to 2019) at : https://www1.lmd.polytechnique.fr/dyned/. From 2000 to 2021, a total of 7038 (respectively 8890) anticyclonic (cyclonic) eddy tracks were retrieved. The asymmetry in eddy numbers is driven by a lifetime difference, anticyclones living noticeably longer, an asymmetry even more marked in the Levantine basin (Barboni et al., 2021).

 ## 2.2   In-situ profiles

A climatological database is created collecting in-situ profiles from the Coriolis Ocean Dataset for Reanalysis (CORA). Delayed-time (CORA-DT, Szekely et al. (2019b)) profiles are recovered from 2000 to 2019 (113486 profiles), and near-real-time (Copernicus-NRT, Copernicus (2021)) profiles are recovered from 2020 to 2021 included using the **history** release (22821 profiles). In addition, some profiles prior to 2020 are not yet released in CORA-DT but available in Copernicus-NRT.
130   This happens in particular when the salinity sensor of an Argo float has abnormal values but the temperature is still correct (by visual inspection and correct quality flag). As the MLD computation can be performed on a temperature profile alone, profiles were also retrieved in NRT mode after careful check, described in Appendix A. This provides an extra 20746 profiles from 2000 to 2019. Spotted duplicates between CORA-DT and Copernicus-NRT are retrieved only from CORA-DT. Complete database then accounts for 157053 profiles in total.

135 ## 3   Methods

3.1   MLD computation
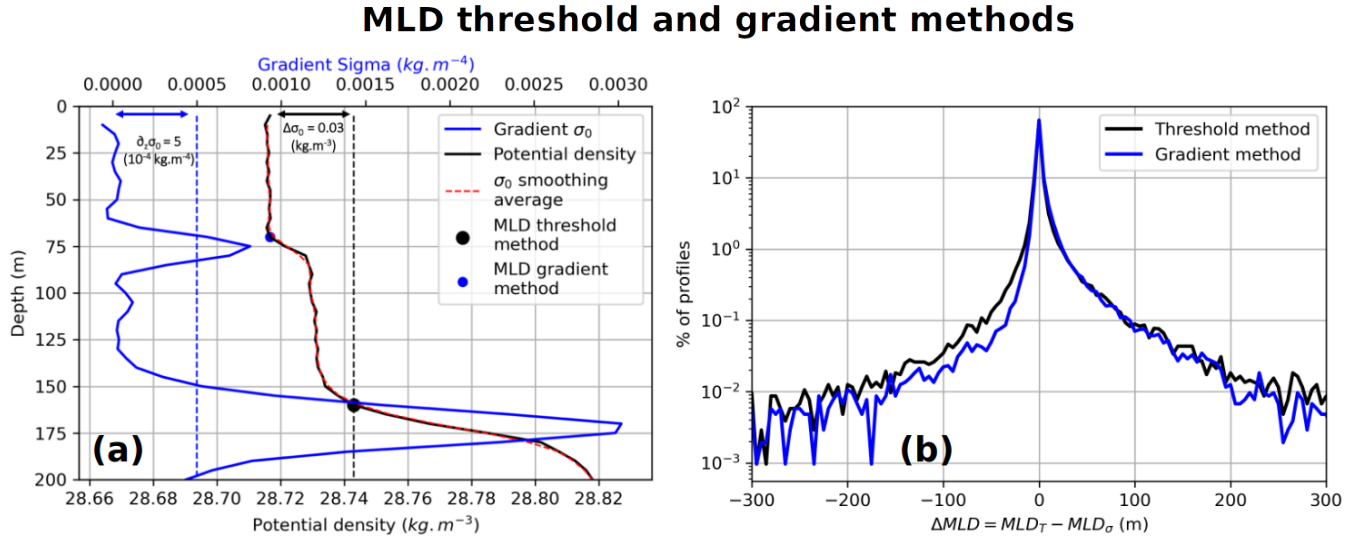
Figure 1. (a) MLD detection on one potential density profile with our gradient method (blue dot) and threshold method (black dot) and (b) fraction of the profiles as a function of ΔMLD for the threshold (black line) and gradient (blue line) method

The global analysis conducted by de Boyer Montégut et al. (2004) led to MLD detected by threshold values of $0.03 kg.m^{-3}$ for density and 0.2°C for temperature, based on a reference depth at 10 m to avoid diurnal heating at the surface. In the Mediter-ranean sea d'Ortenzio et al. (2005) used this methodology for a 0.5°resolution MLD climatology. Houpert et al. (2015) updated
140   it with 8 supplementary years of data, but opted for a 0.1°C temperature threshold. This more restrictive criterion enables to

reduce the difference between the MLD computed on temperature profiles with the one on density profiles. Gradient methods are looking in a similar way for critical gradients as an indicator of the mixed layer base. Typical gradient threshold values in use are $2.5 \times 10^{-2}\,°C\,m^{-1}$ for temperature profiles and range from 5×10^{-4} to $5 \times 10^{-2}\,kg.m^{-4}$ for potential density profiles (Dong et al., 2008). Mixed gradient and threshold methods were also developed (Holte and Talley, 2009). Here we aim to capture as accurately as possible the MLD evolution, which can vary on timescales shorter than a month. More specifically we observed in several cases that the threshold method (with criteria $\Delta\sigma = 0.03\,kg.m^{-3}$ and $\Delta T = 0.1$ °C) can miss the mixed layer and return the main thermocline instead (see Fig.1a). The main thermocline is indeed characterized by a small jump in potential density (or in temperature) but a significant peak in the gradient profile, and happens mostly in the spring, probably due to a start of restratification quickly mixed. To capture such small-scale restratification events, we built the following methodology combining both threshold and gradient approaches. Using the following thresholds : $\Delta\sigma = 0.03\,kg.m^{-3}$ and $\Delta T = 0.1$ °C, we derive a first estimate of the MLD. If it is shallower than 20 m, we take it as our estimate of the MLD. Otherwise, we apply a three-point running average to remove small spikes and compute the gradient using a second-order centered difference. From the subsurface (20 m) up to the first MLD estimate, we apply a gradient method with the given gradient thresholds : $|\partial_z\sigma| > 5 \times 10^{-4}\,kg.m^{-4}$ or $|\partial_z T| > 2.5\,°C.m^{-1}$. If the gradient fails to exceed the threshold within the given depth range, then the first MLD estimate is kept.

Threshold and gradient methods are limited by their dependence on the criterion values which can have strong influence on the MLD estimate. The relatively low gradient thresholds chosen here appeared to be necessary to catch the MLD in some of our profiles as higher thresholds would return the main thermocline (see Fig.1a). A sample of 400 randomly-picked profiles colocated inside eddies was used for validation. We chose this validation dataset with profiles inside eddies as it is our main focus. Wrong detection on double gradient profiles inside eddies were found to be quite large, exceeding 100m sometimes. On these 400 profiles, 22 (5.5 %) of them were identified as double gradient profiles, resulting in an overestimated MLD when derived with the threshold method. Moving to our methodology, this issue is now only encountered for 2 profiles (0.5 %). However, with the gradient method comes some issues on profiles with small residual spikes despite the applied smoothing. For 2 profiles, the gradient method returned wrong MLD detection where the threshold method was correct. However, the gradient method was found overall to be more accurate on estimating the MLD.

Moreover the chosen thresholds should return similar estimates between a MLD obtained from temperature profile (MLD_T) and one from a potential density profile (MLD_σ). Potential density is a better estimate of the stability of a layer, and thus MLD_σ should give a more reliable value. However, salinity (and hence density) suffers from data holes, representing about 15 % in our dataset. Temperature profiles then offer a good alternative in evaluating the MLD providing MLD_T gives similar a estimate than MLD_σ. MLD_T and MLD_σ difference histogram is shown in Fig.1b: the gradient method appears to slightly reduce this difference with 64 % of the profiles leading to the same estimate and 94 % to less than a 30 m difference compare to 62 and 93 % respectively for the threshold method. MLD is then computed on the density profile, and on the temperature if no density is available.

3.2 Eddy colocalisation and background estimate
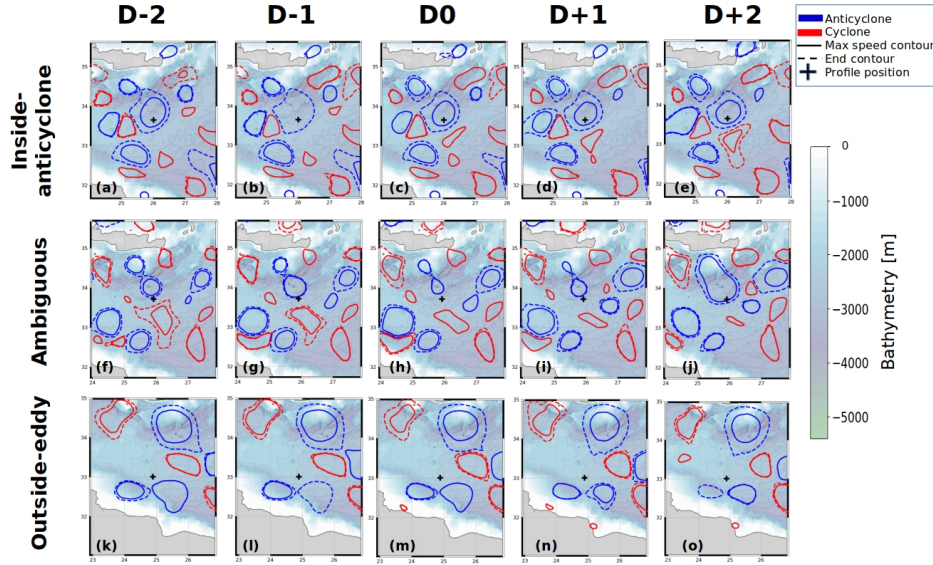
Figure 2. Profiles colocalisation with eddy contours for an 'inside-anticyclone' profile (panels (a) to (e)), an 'ambiguous' profile (panels (f) to (j)) and an 'outside-eddy' profile (panels (k) to (o)). Profile cast position is assumed fixed and compared to eddy contours at D-2, D-1, D, D+1, D+2, D being the profile cast date.

In order to characterize the impact of anticyclonic eddies on the MLD seasonal evolution and spatial gradient, we need to accurately colocalize in situ profiles with eddy observations. However due to altimetric product interpolation and disparate satellite tracks, SSH-based contours can vary a lot in size and position, making a single eddy observation less reliable in the Mediterranean sea (Amores et al., 2019; Stegner et al., 2021). Therefore we colocalize eddy observations and in situ profiles at ±2 days. Assuming a profile position fixed at cast date D, it is then labeled as 'inside-eddy' if it remains inside the maximal speed contours of the same eddy at D-2, D-1, D, D+1 and D+2 (at least 4 contours out of 5). This 4-out-of-5 threshold avoids to neglect a colocated profile when the eddy contour is not available for just one day (see Fig.2b). For the same purpose, hereafter the eddy center and the distance of a profile to the eddy center are averaged at ±2 days.

AMEDA also gives for each observation the last closed SSH contour (see section 2.1), inside which there is still an impact of the eddy shear, but outside of the maximal speed contour the water particles are not assumed to be trapped. The area between the maximal speed and last closed SSH contours are then considered as an intermediate zone to be discarded. Consistently with the 'inside-eddy' definition, we label as 'outside-eddy' only profiles staying outside any eddy contours at ±2 days of its cast date. Any profile being neither 'inside-' or 'outside-eddy' is considered as ambiguous and discarded. From 2000 to 2021, out of 157053 profiles retrieved in the Mediterranean sea, 104787 are labelled 'outside-eddy', 7939 are 'inside-anticyclone', 14919

'inside-cyclone', and the remaining 29410 'ambiguous' profiles are removed from this analysis. This asymmetry between anticyclones and cyclones sampling is also due to heterogeneous oceanographic surveys (Houpert et al., 2015), in particular the numerous glider missions in the Gulf of Lion, a cyclonic gyre with no large anticyclones (Millot and Taupier-Letage, 2005). Figure 2 illustrates the colocalisation method detailed above with 3 examples : an 'inside-anticyclone' profile (Fig.2a-e), an 'ambiguous' one (Fig.2f-j) and an 'outside-eddy' one (Fig.2k-o). For this particular 'inside-anticyclone' profile, the maximal speed contour was missing at day D-1, but available the other days, and the profile was indeed cast close to the eddy center.

To follow the accurate evolution of the MLD inside anticyclones, we need a reference for comparison: an unperturbed, local and time-coincident ocean state without eddies, hereafter called 'background'. This outside-eddy background differs from a classical climatology used in previous studies (Gaube et al., 2019) by removing the eddy mean effect and by avoiding as much as possible time-averaging. The background of an eddy, at a given time t and center position $C(t)$, is then constituted by the mean of all profiles labelled as outside-eddy closer than 250km from $C(t)$, cast within $\Delta day = \pm 10$ days of the same year, or the previous or the following year ($\Delta y = \pm 1$ year). For example when computing the corresponding background of an eddy around 15 February 2018, the background encompasses profiles labelled 'outside-eddy', closer than 250km and cast from 5 to 25 February 2017, 2018 and 2019. A threshold on the number of profiles is required : if less than 10 profiles meet the distance, time and outside-eddy requirements, then no background is computed. At last we define as 'background MLD' the median MLD of the profiles constituting the background. Computing the median is preferred to the mean as the MLD distribution is not centered, being only towards the bottom. This computation is performed for each timestep, with temporal resolution of 5 days. As shown in Appendix (Fig.A1), with the test case of the Ierapetra anticyclone over 2 years (corresponding events 'IER1-2' on Table1 and Fig.10), the background MLD is not highly sensitive to the choice of Δday and Δy. The background MLD evolution is indeed similar with $\Delta day = 10, 15$ or 20 days and $\Delta y = 0, 1$ or 2 years. It is however important not to take all years, as interannual variability then starts to smooth the background MLD evolution. On the other hand taking only profiles of the same year ($\Delta y = 0$) sometimes translates in not enough profiles to have a background estimate (see Fig.A1a). We therefore chose $\Delta day = 10$ days and $\Delta y = 1$ year as day and year intervals in order to capture MLD variation as short as possible, which is crucial for parameters varying quickly such as the MLD. For the two earliest recorded events (Mersa-Matruh 1 and 2 in 2006 and in 2008, see Table1), Δy is set to 2 years because no background MLD was available otherwise. Choosing $\Delta y = 1$ allows to have accurate eddy induced anomalies without being corrupted by interannual variability of temperature and salinity fields, which can be marked in the Mediterranean, in particular in the Eastern basin (Ozer et al., 2017) and with a significant warming trend (Parras-Berrocal et al., 2020).

3.3 MLD evolution function fit

To describe more objectively the MLD seasonal evolution in the background, we performed a function fit using the Python optimization routine `scipy.optimize.curve_fit`. MLD data points are selected per 5 days time steps. Background MLD is fitted by a skewed Gaussian, t_{max}^{back} being the time when deepest MLD (MLD_{max}^{back}) is reached, σ and τ respectively the
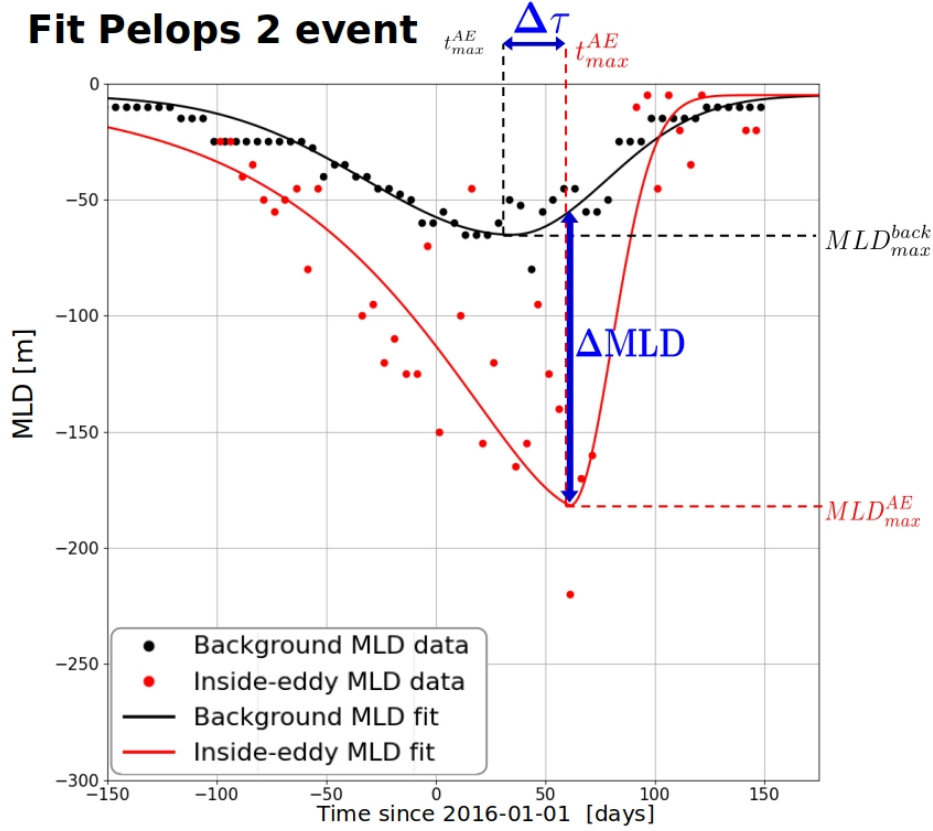
Figure 3. Detail of winter deepening event Pelops (PEL) 2 in 2016 (see Table1 for details). Anticyclonic core MLD data are shown as red dots, background MLD as black dots, with time steps of 5 days. MLD fit is shown as a red line for the anticyclonic core (see Eq.2) and as a black line for background MLD (see Eq.1).

225   deepening and restratification timescales :

$$
\begin{aligned}
f(t) &= MLD_{max}^{back} \exp\left(-\frac{(t - t_{max}^{back})^2}{2\tau^2}\right) && \text{if } t > t_{max}^{back} \\
f(t) &= MLD_{max}^{back} \exp\left(-\frac{(t - t_{max}^{back})^2}{2\sigma^2}\right) && \text{otherwise}
\end{aligned}
\tag{1}
$$

This fit captures the background MLD evolution, somehow smooth, typically with a sharper restratification than deepening ($\tau < \sigma$). However this is not sufficient for the anticyclonic core MLD evolution that can have more abrupt variations, then calling for a more complex fit with two deepening timescales σ_1 and σ_2 :

230

$$
\begin{aligned}
f(t) &= \left(MLD_{max}^{AE} - B\right) \exp\left(\frac{t - t_{max}^{AE}}{\tau_1}\right) + B \exp\left(\frac{t - t_{max}^{AE}}{\tau_2}\right) && \text{if } t > t_{max}^{AE} \\
f(t) &= MLD_{max}^{AE} \exp\left(-\frac{(t - t_{max}^{AE})^2}{2\sigma^2}\right) && \text{otherwise}
\end{aligned}
\tag{2}
$$

To fit accurately the MLD evolution, and in particular the maximal depth reached, data are fitted with weights proportional to their depth. Because it is difficult to have long and continuous time series, data are often missing on the previous or next summers. To ensure physical behavior, fit is forced back to 10m on the edges, miming summer stratification. The MLD anomaly (MLD^{anom}) is defined as the difference between the fitted background and anticyclonic core MLD. MLD^{anom} is a function of time but reaches its maximum (ΔMLD) at almost the same time than the absolute anticyclonic core MLD, as the latter has more amplitude than the background one. At last an advantage of the `scipy.optimize.curve_fit` routine is to provide the parameter covariance matrix, and hence an error estimate taking the square root of the covariance matrix diagonal (Bevington et al., 1993). It can happen for the covariance matrix to have very large values, in this case we used an upper uncertainty of $\pm30m$ for ΔMLD and ±20 days for t_{max}^{AE}. A fit illustration is provided in Fig.3 for the Pelops 2 event in 2016 (see Table1), with dots as the real MLD data and fits in continuous lines, background in black and anticyclonic core in red. Using the fit routine, maximal MLD anomaly is then estimated for this event to $\Delta MLD = 127 \pm 13\,m$. On can also notice an absence of coincidence between deepest inside-eddy and background MLDs. Following previous notation, we can then define a restratification delay of the anticyclonic core MLD, used throughout this study : $\Delta \tau = t_{max}^{AE} - t_{max}^{back}$. In the example shown in Fig.3, $\Delta \tau = 26 \pm 11$ days.

4 Results

Several long-lived anticyclones are tracked for several months, recording up to 16 winter mixed layer deepening events at their core. In order to investigate the relation between the MLD evolution and the vertical eddy structure, we plot together the timeseries of MLD and vertical temperature gradients inside the eddy core. Two different MLD temporal patterns are observed, depending on whether or not the current winter mixed layer reaches the subsurface anticyclone core. This core is constituted by a preexisting homogeneous layer, and in the following, we define as 'homogenized' a layer with temperature gradient constantly below $2.5 \times 10^{-3}\,°C.m^{-1}$ in absolute value.

4.1 Winter deepening connecting preexisting subsurface core

Very deep mixed layer can be observed in several anticyclones when the MLD erodes the inside-eddy stratification and abruptly connects with a subsurface homogenized core, an event hereafter called a 'connecting' MLD. An example of this evolution is described below with a long-lived Eratosthenes anticyclone during winter 2008-2009. Its temporal evolution from August 2007 to April 2009 is shown in Fig.4, and listed hereafter and in Table1 with name 'Eratosthenes (ERA) 1'. This kind of anticyclone, also called 'Cyprus eddy' or even 'Shikmonah gyre', are large mesoscale structures with almost stationary position south of Cyprus island in the Levantine basin, extensively studied with several CTDs (Brenner, 1993; Krom et al., 1992; Moutin and Prieur, 2012), gliders and Argo floats deployments (Hayes et al., 2011). The anticyclonic density anomaly is characterized on average by a deep (about 400m) and extremely warm temperature anomaly (up to +2°C at 400m) (Moutin and Prieur, 2012; Barboni et al., 2021), sometimes with a strong salt anomaly (Hayes et al., 2011). Thus temperature profiles are considered as a
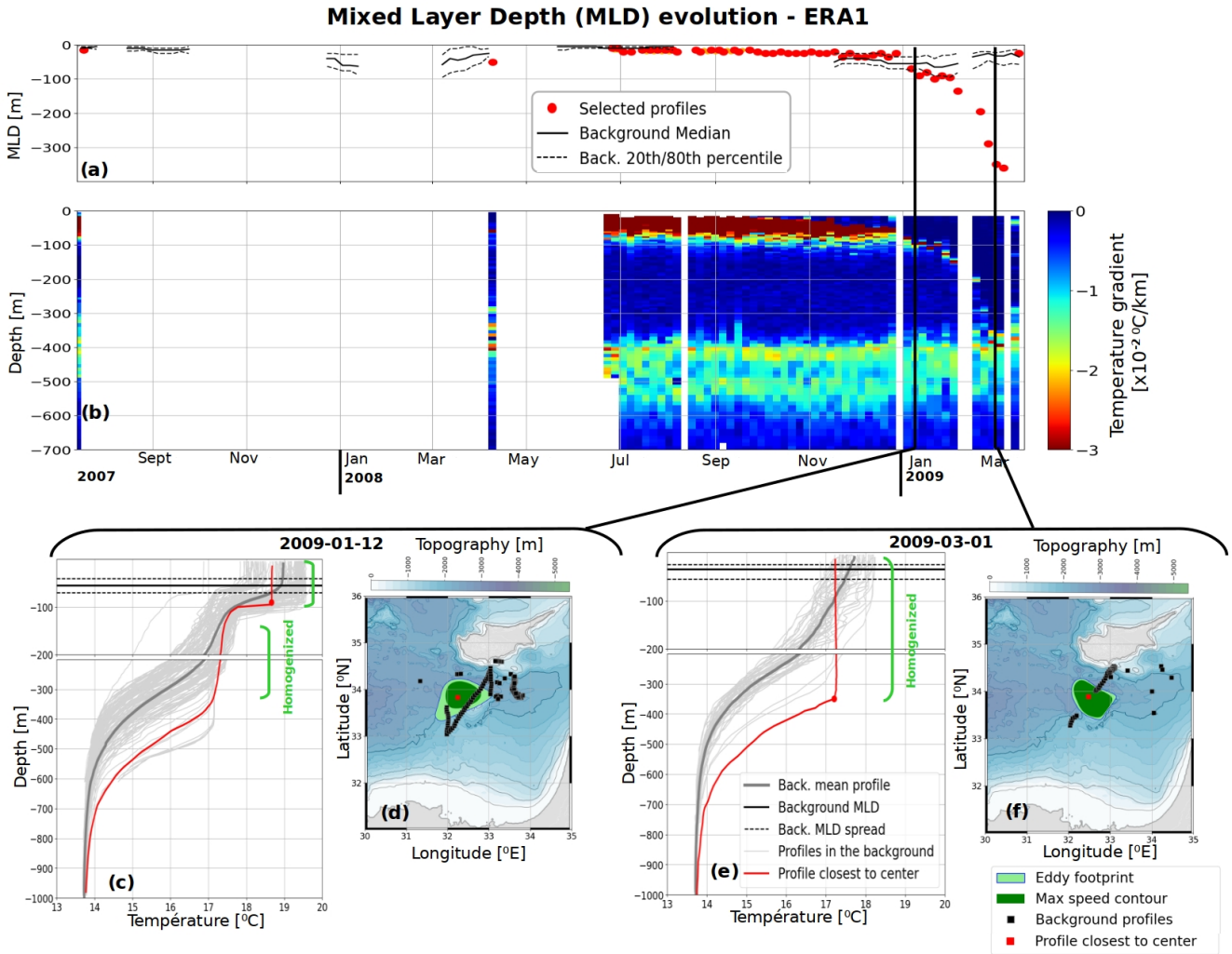
Figure 4. In depth evolution of a Eratosthenes anticyclone, listed as 'ERA1' in Table1. (a) MLD evolution, with black continuous line for background MLD (and dashed line for associated spread between 20th and 80th percentiles), anticyclonic core MLD closest to eddy center with red dots. (b) Time series of inside-eddy temperature gradient, blue showing homogeneous and red stratified layers. (c) (respectively (e)) shows vertical profiles around 12 January 2009 (1 March 2009) with background profiles in thin gray lines, background mean as thick gray line, inside-eddy profile as red line, a red dot highlighting anticyclonic core MLD and a green bar indicating homogenized layers (temperature gradient below $2.5 \times 10^{-3}\ ^{\circ}C.m^{-1}$). Horizontal continuous and dashed black line reminds background MLD and spread from panel (a). (d) (respectively (f)) shows profiles corresponding position on a map with same color code, together with the eddy maximal speed contour (dark green green shape) and eddy footprint (outermost closed SSH contour, light green shape). Bathymetric data are from ETOPO1 (Smith and Sandwell, 1997).

good estimate for relative density and temperature gradient for stratification.

An Argo float remained trapped inside this anticyclone from mid-2008 to the death of this eddy in early 2009, allowing to capture well an MLD deepening event during winter 2008-2009. An inside-anticyclone profile is shown at the beginning (12 January 2009, Fig.4c) and the end (1 March 2009, Fig.4e) of the winter. First one can notice that the anticyclone vertical structure in January 2009 is constituted by a subsurface homogenized layer from 100 to 300m, which can be tracked since July 2008 on the stratification timeseries (Fig.4b) and likely formed by convection in the previous winter. Anticyclone core profile on Fig.4c has indeed a marked temperature anomaly on the order of $+2°C$ at 450m compared to the background, proving they indeed sample the eddy core. Some profiles with very warm temperature at 400m deep are misleadingly considered as outside-eddy but do not corrupt the mean background (thick gray line). MLD is also deeper inside the Eratosthenes anticyclone : the anticyclonic core MLD is 90m deep, while it is around 60m in the background. The deeper homogenized core remaining unmixed below a seasonal thermocline : $+1$ °C temperature jump at 100m on Fig.4c. Later, the winter cooling and subsequent MLD deepening eroded this stratification inside the anticyclone, as shown by the temperature gradient vanishing in the upper 100m, and the winter MLD connects with the primitive core and mix it in February 2009 (Fig.4b). Then on 1 March 2009 (Fig.4e) the anticyclone core profile measured a MLD reaching 350m.

MLD temporal evolution noticeably do not coincide inside- and outside-eddy : on MLD timeseries (Fig.4a) background MLD shoaled since end of January, whereas inside-eddy MLD continued to deepen. Then on 1 March 2009 most background profiles started to restratify with temperature gradient in the upper 100m (thin gray lines in Fig.4e), while anticyclonic core MLD rose back to about 20m only in late March 2009 (Fig.4a). This restratification occurring at a different time outside- and inside-eddy - with a delay of about two months - leads to the noticeable situation measured on 1 March 2009 : the inside-anticyclone profile is warmer than its environment at depth (100 to 350m deep) but homogenized in its upper part, whereas background profiles are stratified with positive temperature gradient. Such geometrical configuration leads to an anticyclone negative temperature (and hence positive density) anomaly from 50m to the surface, compared to the stratified outside-eddy profile. Such positive density anomaly above the eddy core is then a clear signature of subsurface anticyclone (Assassi et al., 2016).

Over the whole 2008-2009 winter, background MLD barely reached 60m whereas the anticyclonic core MLD went down to 350m. This intense deepening at the anticyclone core is due to the preexisting subsurface eddy, made of a well mixed layer of few hundred meter depth below the summer stratification. When the winter mixed layer deepens, it reconnects to this deep sub-surface core and leads to a rapid and strong MLD increase in comparison to the eddy background. This MLD temporal pattern is characteristic of a 'connecting' event, observed 10 times in our analysis and throughout the Mediterranean sea (see section 4.3).

4.2 Winter deepening not connecting preexisting subsurface core

Conversely for some other anticyclones, it can clearly be seen that the subsurface temperature anomaly does not connect with the winter mixed layer and remains unperturbed and homogeneized at depth. Such event is hereafter called a 'non-connecting'
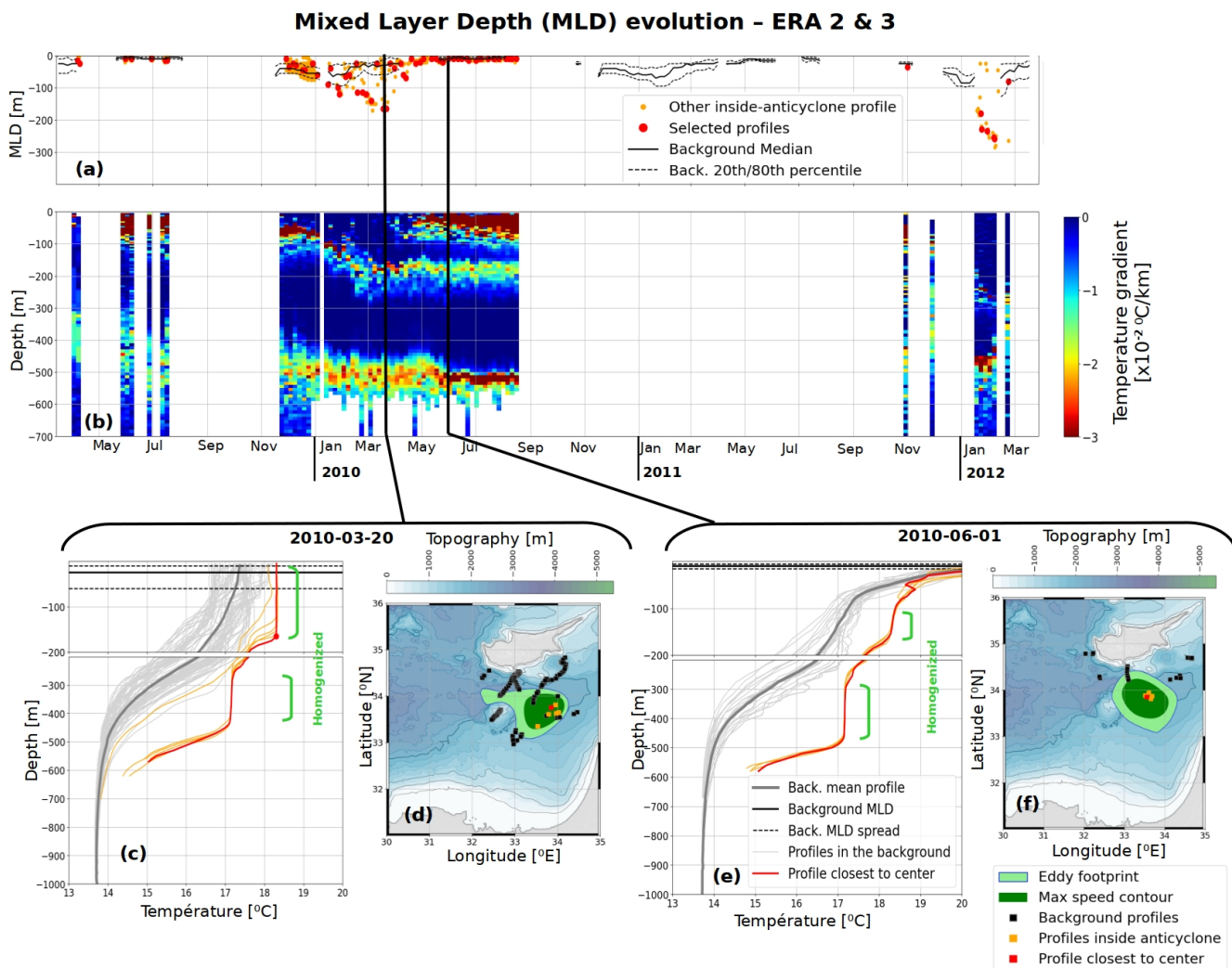
Figure 5. Same color codes and legend as in Fig.4. In panel (a),(c) and (e), orange lines and dots show additional inside-eddy profiles and corresponding MLD, but further away from eddy center than the selected one shown in red.

MLD. Figure 5 shows the evolution of another Eratosthenes anticyclone living from 2009 to early 2012, with two recorded anticyclonic core MLD deepening in 2010 and 2012 (respectively listed in Table1 as 'ERA2' and 'ERA3'), with same color codes than Fig.4, with profiles at 20 March 2010 and 15 June 2010. As several profiles were located at the same time inside the anticyclone, they are shown in orange line on Fig.5c and 5e (respectively orange dot for MLD on Fig.5a). The red line highlights only the profile with closest distance to the eddy center, assumed to be more representative of the eddy core.

300

Similarly to the 'ERA1' event in 2009 described above, a thick and deep subsurface anomaly forms primitive eddy core in late 2009, as an homogeneous layer from 250 to 400m deep (green bar on Fig. 5c), reaching an anomaly about +2.5°C at 400m. However the anticyclonic core MLD did not deepened in the winter 2009-2010 below 150m, only forming a second homogeneous layer above. This constitutes a second surface core, still separated from the primitive core by a temperature stratification, revealed by a temperature gradient continuous in time (Fig.5b). On the vertical profile on 20 March 2010 (Fig.5c) about 1°C temperature jump remains between the two core, forming a double-core anticyclone. In June 2010 (Fig.5e), this second homogeneous layer is itself covered by the spring restratification, then forming what is also referred to as 'thermostad', or 'mode-water eddy' in the literature (Dugan et al., 1982). Thanks to the trapped Argo floats remaining near the eddy core for months, both cores can be tracked until August 2010 as separated in subsurface.

Such 'non-connecting' winter MLD inside anticyclone reveals the possibility of a persisting separation between a primitive subsurface anticyclone core and the new homogeneous layer formed by the current winter mixing, then constituting a double-core anticyclone. The example showed in Fig.5 occurred on a Eratosthenes anticyclone, in the same region than anticyclone in which a 'connecting' MLD example was previously shwon in Fig.4. This MLD pattern is not limited to this example and was also observed 5 times in other regions, as detailed in the next section. Consequences of the formation of a double-core anticyclone are discussed in Sect.5.2 hereafter, with another remarkable example in Fig.10.

4.3 Inside-anticyclone MLD statistics

From 2000 to 2021, thanks to extensive Argo deployments sampling eddies, 16 winter MLD deepening events were accurately recorded with vertical profiles in 13 mesoscale eddies, 10 being 'connecting' events, 6 'non-connecting' ones. Several structures were indeed surveyed over 2 winters (see Fig.5 and 10). For each event, the fitting method detailed in Sect.3.3 is applied and parameters are reported in Table1 together with eddy characteristics : eddy SSH amplitude, maximal speed V_{max} and maximal speed radius R_{max}. Eddy measurements are estimated by the mean from November to March of the corresponding winter. Figure 6 shows the location of each structure, which actually corresponds to a type of long-lived structures already identified in the literature (Millot and Taupier-Letage, 2005; Hamad et al., 2006; Budillon et al., 2009; Barboni et al., 2021), from West to East : Central Tyrrhenian anticyclone (abbreviated TYR), Pelops (PEL), Ierapetra (IER), Mersa-Matruh (MM) and Eratosthenes (ERA). Position is computed as the mean position during the corresponding winter, even though eddies do not drift a lot in the Mediterranean sea (Mkhinini et al., 2014). Despite regional differences and limited data availability, both types can occur in each region, and provide an observation database allowing statistical comparison. Inside-eddy maximal MLD time t_{max}^{AE} and hence $\Delta \tau$ could not be computed for events MM4 and PEL3, as gaps in the time series do not allow to accurately measure them. However ΔMLD could always be computed as in worst cases there are still inside-eddy profiles later in the year allowing to check that maximal MLD was indeed reached (in similar way than Moutin and Prieur (2012) for previous winter MLD retrieved in April). Both types of events entail interaction (or not) with a deep surface homogeneous layer (layer with temperature gradient below 2.5×10^{-3} °$C.m^{-1}$ in absolute value), either a preexisting one (see Fig.4c, 4c and
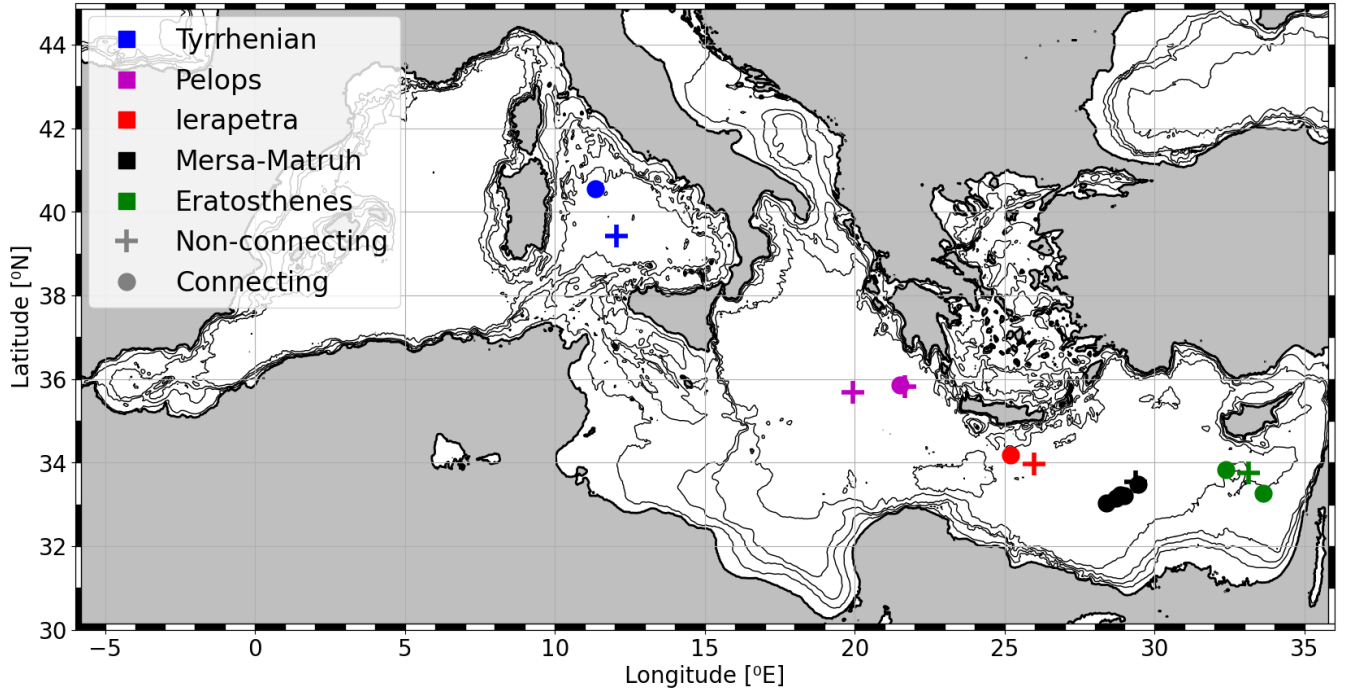
Figure 6. Map of well-sampled winter mixed layer deepening events inside anticyclones listed in Table1. Big dots show 'connecting' events, while crosses show 'non-connecting' ones. Color depends on the region : Central Tyrrhenian (TYR), Pelops (PEL), Ierapetra (IER), Mersa-Matruh (MM) and Eratosthenes (ERA, also called "Cyprus"). Isobaths shown on the maps are at 100, 500, 1000 and 1500m depth, topographic data from ETOPO1 (Smith and Sandwell, 1997).

10c) or a new one (see Fig.5e and 10d). In all winter deepening events listed on Table 1, such homogeneous layers of least 50m were indeed visible on vertical profiles. For Tyrrhenian sea anticyclones (TYR1 & 2) with stronger salinity influence (Budillon
340 et al., 2009), homogeneous layers with density gradient below $5.0 \times 10^{-4} \, kg.m^{-4}$ are also visible. One can also notice that 'non-connecting' events are quite common, but double-core structures should be even more frequent. Indeed a 'connecting' event can occur inside a double-core structure and reconnect only the homogeneous core formed in the previous winter but not the deepest anomaly, as shown later in Fig.10b-e. In other worlds the proportion of 'non-connecting' events in Table 1 and Fig.6 should be considered as a lower bound for double-core structures, revealing their high occurrence.

345

Hausmann et al. (2017) and Gaube et al. (2019) proposed a linear relation between the anticyclonic core MLD anomaly and its SSH amplitude, using regional average and monthly climatology. We previously showed that MLD anomaly varying over very short timescales can produce sharp MLD gradient and anomalies reaching several hundreds meters, not captured by smoothed composites. The relation between MLD anomaly and eddy amplitude is tested on Fig.7a, distinguishing 'connect-
350 ing' (red dots) and 'non-connecting' (green dots) events, together with Gaube et al. (2019) relation in dashed line (1m MLD

Table 1. Main characteristics of the 16 anticyclonic core mixed layer deepening events studied, fitting method and uncertainties are detailed in Sect.3.3. Eddy ID refers to track number in the DYNED Atlas. Event types are 'C' for 'connecting' and 'N' for 'non-connecting'. Year '2018' corresponds to winter 2017-2018. Regions codes, ordered from West to East, stand for : Central Tyrrhenian (TYR), Pelops (PEL), Ierapetra (IER), Mersa-Matruh (MM) and Eratosthenes (ERA). ΔMLD, t_{max}^{AE} and $\Delta\tau$ are illustrated on Fig.3. Note that sometimes two different winters are recorded in the same anticyclone (for example 'IER 1-2'), and that one eddy tracking ('MM 6') stopped because the dataset finished in December 2021.

Event	Eddy ID	Type	Year	Position (°N ; °E)	ΔMLD (m)	t_{max}^{AE} (days since 1 January)	$\Delta\tau$ (days)	Amplitude (cm)	R_{max} (km)	V_{max} (m.s^{-1})	Eddy lifetime (days)
TYR1	11780	C	2018	40.6 ; 11.3	255± 15	50± 3	17± 4	5.5±0.9	38.3±4.3	0.24±0.02	498
TYR2	12976	N	2020	39.4 ; 12.0	49± 4	28± 4	4± 5	7.2±3.4	33.4±2.6	0.18±0.02	541
PEL1	8886	N	2015	35.7 ; 19.9	196± 7	79± 4	62± 5	4.2±0.9	42.0±8.7	0.19±0.04	756
PEL2	10054	N	2016	35.8 ; 21.7	127± 13	61± 10	26± 11	6.3±1.7	38.1±8.7	0.31±0.07	578
PEL3	11649	C	2019	35.9 ; 21.5	79± 23	-	-	7.8±0.9	39.3±6.6	0.36±0.04	1010
IER1	11099	N	2017	34.0 ; 26.0	175± 41	67± 20	46± 20	7.7±1.1	37.3±4.3	0.41±0.05	780
IER2	11099	C	2018	34.2 ; 25.2	211± 12	51± 4	16± 6	7.4±1.6	40.9±6.9	0.35±0.07	780
MM1	3556	C	2006	33.1 ; 28.7	197± 30	40± 20	13± 20	9.3±1.2	45.4±7.5	0.41±0.06	345
MM2	4125	C	2008	33.5 ; 29.4	325± 12	47± 2	36± 8	3.7±0.7	37.7±5.7	0.20±0.04	790
MM3	7656	C	2015	33.2 ; 28.8	236± 7	38± 2	42± 5	8.6±2.2	47.8±9.3	0.35±0.04	1229
MM4	11544	C	2018	33.2 ; 29.0	187± 30	-	-	11.4±1.6	61.0±10.0	0.38±0.04	1045
MM5	11544	C	2019	33.0 ; 28.4	215± 30	29± 20	13± 20	8.7±0.9	43.0±4.6	0.41±0.05	1045
MM6	14400	N	2021	33.5 ; 29.4	151± 12	80± 5	74± 7	3.1±1.1	35.9±7.0	0.18±0.03	476+
ERA1	4914	C	2009	33.8 ; 32.4	338± 30	62± 5	39± 7	2.1±1.0	34.9±7.8	0.12±0.04	616
ERA2	5906	N	2010	33.8 ; 33.1	136± 7	76± 4	67± 8	3.2±2.0	40.1±13.6	0.16±0.08	1110
ERA3	5906	C	2012	33.3 ; 33.6	180± 30	37± 20	13± 20	4.6±1.0	41.8±5.8	0.22±0.04	1110

anomaly for 1cm eddy amplitude). This proposed relation is obviously not verified, the deep MLD observed in Mediterranean anticyclones exceeding by far the relation. On the opposite, deepest MLD anomalies seem to be observed in the eddies with weakest SSH signature. Although surprising at first sight, this trend might be explained by the fact that deepest MLD can be observed when mixed layer abruptly connects to an anticyclone deep homogeneous core, in subsurface and hidden by a strong seasonal thermocline. This is in particular the case for 'ERA1' shown in Fig.4, having an extreme ΔMLD deeper than 300m but the lowest SSH signature in Table 1.
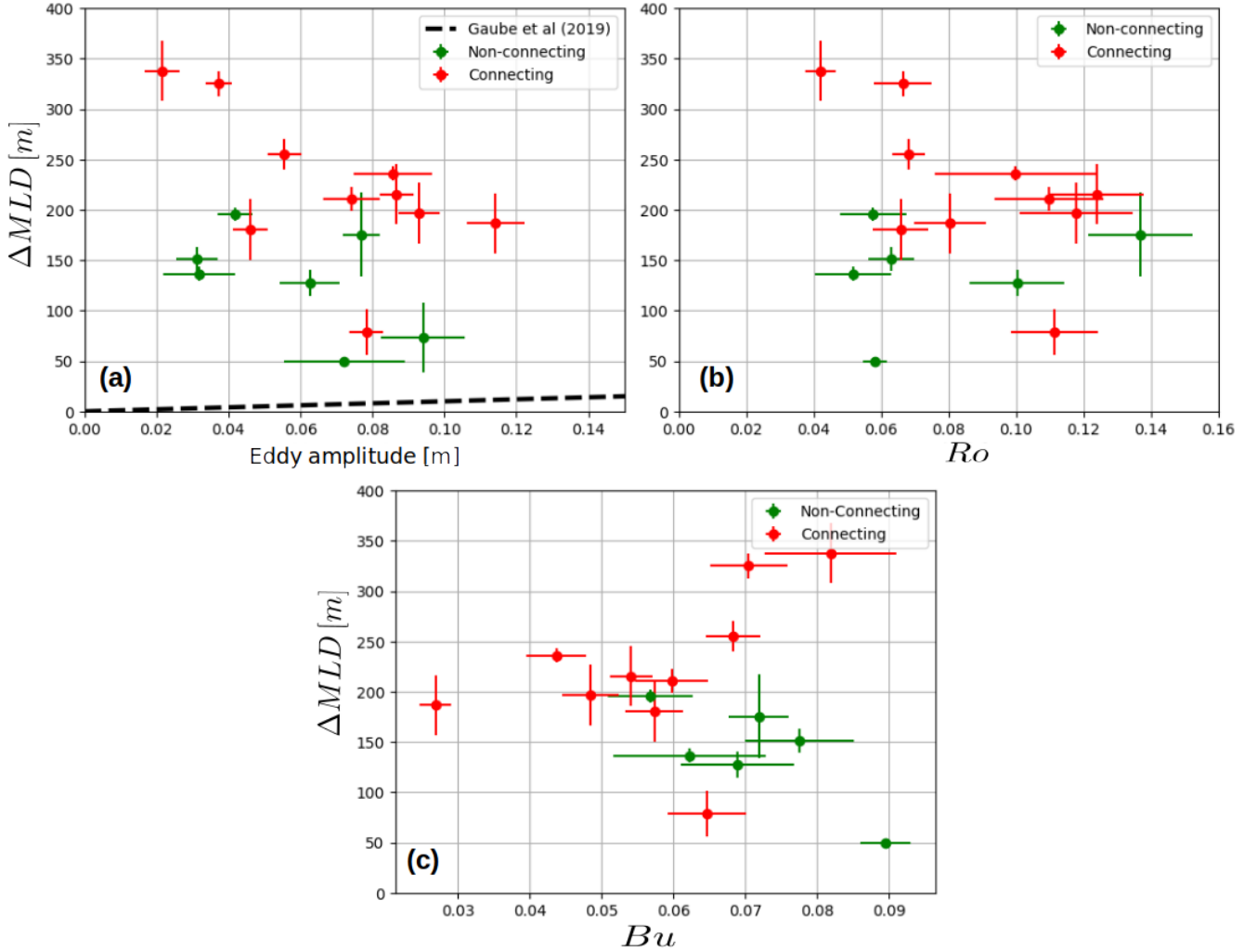
Figure 7. Relationship between maximal MLD anomaly (ΔMLD) and eddy parameters possibly measured through remote sensing : (a) eddy SSH amplitude, compared with proposed 1m MLD for 1cm SSH relation (Gaube et al., 2019), (b) Rossby number (eddy intensity), and (c) Burger number (non-dimensional eddy size).

The relation between the MLD anomaly and the eddy Rossby and Burger numbers are also tested in Fig.7b and 7c. Rossby number, defined as $Ro = V_{max}/fR_{max}$ where f is the Coriolis frequency, is a non-dimensional measurement of the eddy intensity. The Burger number, defined as $Bu = (R_d/R_{max})^2$ with R_d the deformation radius (8 to 12 km in the Mediterranean sea) is a non-dimensional eddy size. Similarly to eddy SSH amplitude, no clear relation can be retrieved, deep and shallow MLD anomalies appear for various eddy intensity and size and for both 'connecting' and 'non-connecting' events. One can only notice that 'connecting' events pull MLD deeper in general, and that these events are slightly more observed in large structures (small Bu). Remote-sensing measurements are then hard to link with observed eddy-induced MLD anomalies. On

360

365   the opposite the diversity of vertical structure shown in this study (Fig.4, 5 and 10) suggests that eddy vertical structure might have more influence, and previously proposed linear relation seem to apply mostly for surface-intensified structures.

4.4   Inside-anticyclone restratification delay
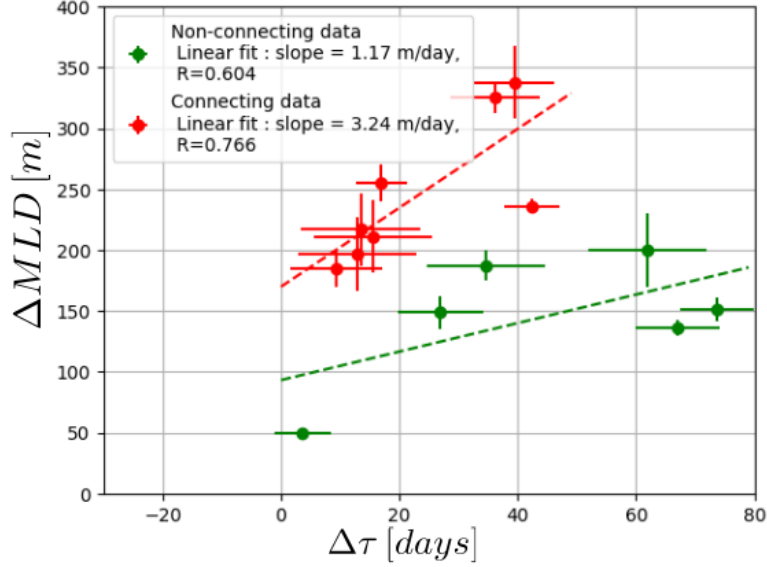
Figure 8. Scaling between the maximal MLD anomaly (ΔMLD) and restratification delay $\Delta\tau$ (see scheme on Fig.3), distinguishing 'connecting' (red) and 'non-connecting' (green) events. Linear fit is applied separately and correlation coefficient put in legend. Data and uncertainty are from Table1.

     A new and important observation is that MLD inside anticyclones tends on average to clearly restratify later than the neigh-
370   bouring background. It was shown for two individual events in Fig.4 (ERA1, 'connecting') and Fig.5 (ERA2,'non-connecting'), but it is statistically robust in Table1 : average t_{max}^{back} is 22 days and average t_{max}^{AE} is 49 days, meaning restratification usually begins in the second half of February in anticyclones, on average one month later than outside-eddy. Restratification delay $\Delta\tau$ can reach two months in some case : 67 days for ERA2 or 74 days for MM6 (see Fig.9b). Figure 8a shows the relation between $\Delta\tau$ and ΔMLD and reveals that no clear trend can be identified alone : deep MLD anomalies are observed when the anti-
375   cyclone MLD restratify early (low $\Delta\tau$) or later (large $\Delta\tau$). However when distinguishing 'connecting' and 'non-connecting' events, a linear trend appears separately : MLD anomalies go deeper as $\Delta\tau$ increases and for similar $\Delta\tau$ value 'connecting' events go deeper. Linear fit is performed separately for both types, shown by dashed line on Fig.8 : for each day of continued MLD deepening inside anticyclones, a 'connecting' (respectively 'non-connecting') MLD gets about 3m deeper with correlation coefficient of 0.766 (1m deeper with correlation 0.604). This trend is logical, as a later restratification (large $\Delta\tau$) lets the
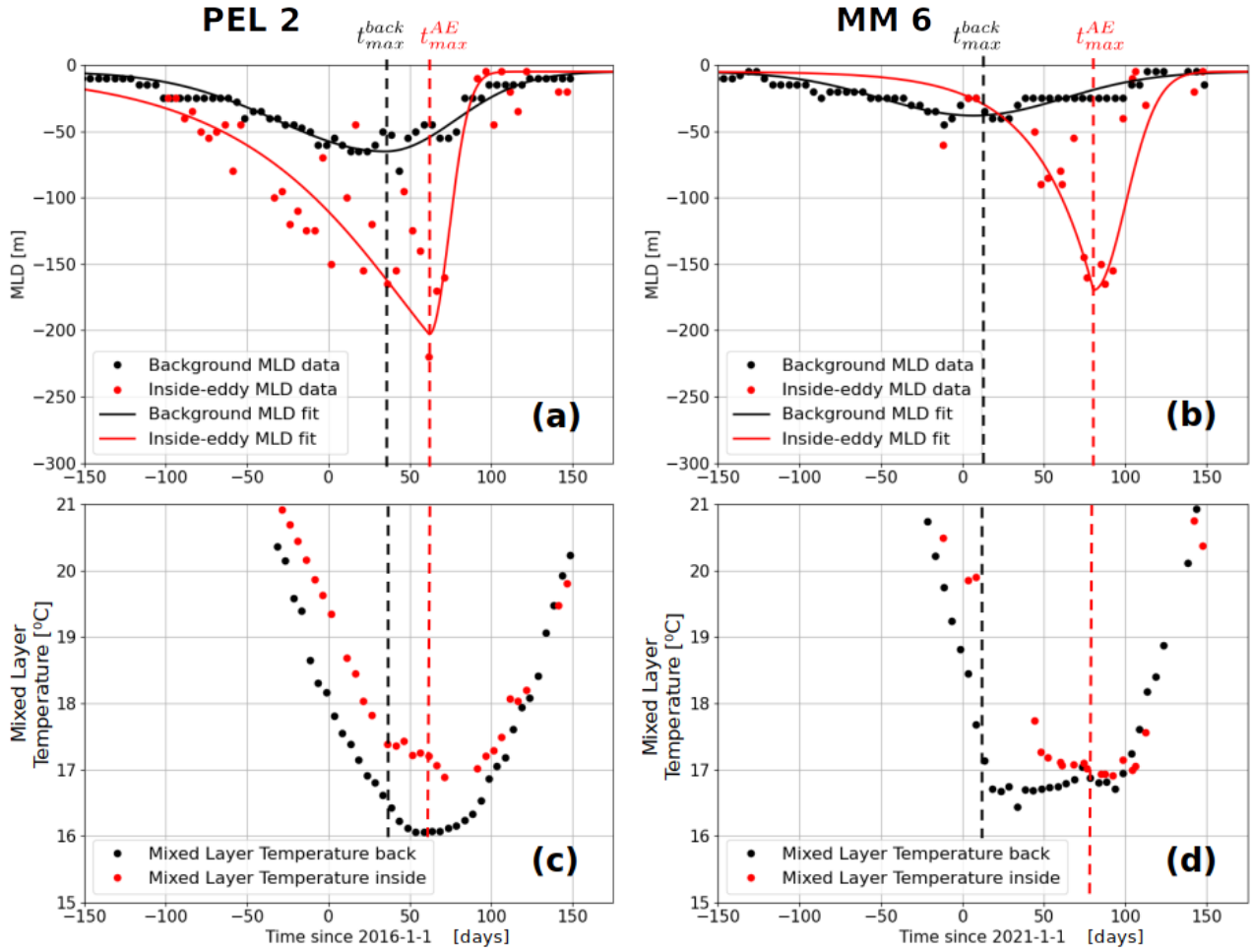
Figure 9. MLD data and fit , inside- and outside-eddy, illustrated for event PEL2 (a) and MM6 (b) (see Table1). In the lower panel corresponding mixed layer temperature evolution for PEL2 (c) and MM6 (d). A black (red) dashed line marks the time of maximal background (inside-eddy) MLD.

380   MLD deepens longer and hence leads to larger ΔMLD.

In order to analyze the MLD evolution together with the mixed layer cooling, Fig.9 shows in the upper panel the MLD fit (see Section 3.3) and in the lower panel the corresponding mixed layer temperature for the PEL2 and MM6 events. Both events are representative of the observed evolution where the temperature can be followed over the whole winter. Maximal background

385   MLD is reached for PEL2 (respectively MM6) around 30 January 2016 (10 January 2021), marking the end of background mixed layer cooling with a plateau temperature of about 16 °C maintained for about 1.5 months (about 16.5 °C for about 3 months) until restratification. In early 2016 (2021), the anticyclone core is indeed about +1°C warmer than its background,

and continues to cool for a while. The inside-eddy maximal MLD is reached around 1 March 2016 (20 March 2021) or +60 (+80) days on Fig.9c (d). Few weeks after, both background and anticyclonic core mixed layers start to warm again around 1 April (in both PEL2 and MM6), but background MLD started to restratify 1 month earlier in PEL2 (2 months earlier in MM6). Although it is hard to infer a mechanism from few observations, it seems that the beginning of restratification outside-eddy does not mean the mixed layer is warmed up again and outside-eddy mixed layer remains cold. The restratification delay seems to be the consequence of a maintained cooling of the initially warmer anticyclone core. Summer heating seems on the other hand to begin at the same time inside- and outside-eddy. Possible mechanism driving this sustained mixing at the anticyclone core are discussed later in section 5.3. An important observation is also that temperature difference between anticyclone core and the background is on the order of $+1°C$ while MLD deepens, but almost vanishes (or even get slightly negative) when the mixed layer warms again. Although sparse, these in situ observation are in total agreement with observed eddy SSTA switch by Moschos et al. (2022) from winter warm-core anticyclones to predominant cold-core anticyclones with spring restratification in the Mediterranean sea.

5 Discussion on physical drivers and perspectives

5.1 MLD anomaly scaling

We clearly identified the distinction between 'connecting' and 'non-connecting' events as a more important driver than other eddy parameters such as eddy amplitude, surface intensity or size (see Fig.7-8), and this might explain the difficulty to find a general law for any eddy-induced MLD anomaly. Indeed 'connecting' deepening mixed layers seem limited by the bottom of the preexisting subsurface homogeneous core to which they connect (example in Fig.4e), whereas 'non-connecting' ones by definition do not go deep enough and are then expected to be limited by the heat loss, likely also influenced by the eddy. The other important parameter is the restratification delay ($\Delta \tau$), measuring how long the anticyclone continues to deepen MLD or not, and which eventually scale with the maximal MLD anomaly. In a remote sensing perspective, both parameters seem very hard to assess without in situ profiles inside the eddies. Examples shown in this study (Fig.4, 5 and 10 below) showed the complexity induced by possible connection with previous subsurface anomaly and more generally the key role of the anticyclone vertical structure, that was totally smoothed in previous composite studies. Relationship between eddy-induced MLD anomaly and satellite measurements are definitely more complex. However as theorized by Assassi et al. (2016), detecting remotely information on the eddy vertical structure could be possible, in particular distinguishing the subsurface or surface-intensified nature by comparing eddy signature in SSH and SST. For instance ERA1 event in Fig.4 is an almost textbook case of a subsurface anticyclone with isopycnals doming leading to a cold eddy-SSTA.

5.2 Double-core eddy formation

High occurrence of 'non-connecting' events (crosses on Fig.6) are very interesting as they show the formation of double-core anticyclones through winter deepening of the surface layer above a preexisting density anomaly. Double-core eddies were often

surveyed in the world ocean (Lilly et al., 2003; Belkin et al., 2020), including in the Western Mediterranean sea (Garreau et al., 2018). Despite various propositions (see e.g. Belkin et al. (2020) for a list), no clear formation mechanisms emerged. Several studies focused on the so-called 'vertical alignment' of two eddies with different densities in experimental works (Nof and Dewar, 1994), observations (Lilly et al., 2003) or modelling (Trodahl et al., 2020). Interestingly Lilly et al. (2003) observed well in the Labrador sea that double-core anticyclones mostly consist of convective lenses formed in different winters, the heat flux interannual variability leading to different density anomalies, but they explained it with eddies formed separately which later aligned. There were nonetheless previous observations of a second lighter core generated above a preexisting anticyclone. Thanks to repeated XBT transects, Nilsson and Cresswell (1980) surveyed such phenomenon in an anticyclone detached from the East Australian Current, caused by winter heat loss. Bosse et al. (2019) surveyed this in the Lofoten eddy with winter convection, but through glider sections spaced in time, then with a temporal resolution on the order of the month. More recently Meunier et al. (2018) explained the formation of a double-core Loop Current Eddy by winter diabatic processes. However this case is different from the Mediterranean anticyclones ; as the Loop Current Eddy consists of an advection of a large structure of Caribbean waters into the Gulf of Mexico experiencing different surface fluxes with more heat loss and precipitation than the area where they originate. These diabatic processes by surface winter mixing result in a fresher shallower core above a saline core of subtropical under waters. Moreover Meunier et al. (2018) explained quantitatively the observed anomaly against regional average of atmospheric fluxes, whereas in our study the differential MLD evolution between the eddy core and the background (Fig.4a and Fig.5a) suggested fluxes variations at the scale of the eddy.

What drives the formation of double-core structures should be further investigated, but one could expect the interannual variability of heat fluxes to be the main driver. This was already suspected by Lilly et al. (2003) (although for them it was for separate eddies) and Moutin and Prieur (2012). A winter with strong heat loss is expected to deepen MLD a lot, including inside-eddy, and a subsequently warmer winter could then not achieve to deepen the MLD as much. This mechanism drives mode-water formation, and it was already shown in other regions, mostly the Atlantic Ocean, that eddies could modulate mode-water formation (Dugan et al., 1982; Chen et al., 2022). Such hypothesis could also explain the high occurrence of 'non-connecting' events in the Mediterranean sea, this region being known for a high interannual variability of winter heat loss. Pettenuzzo et al. (2010) indeed found maximal winter heat loss to vary by 20% to 30% (in regional monthly average), and a plausible connection with the Northern Atlantic Oscillation (NAO). This interannual variability of the heat flux was already shown to influence deep convection in the North-Western Mediterranean sea (L'Hévéder et al., 2013), and it could then be expected a higher occurrence of double-core anticyclones due to a stronger Mediterranean sea stratification in a warming climate (Somot et al., 2006).

An important consequence in the formation of this lighter core in a 'non-connecting' winter deepening is that the second core is separated from the surface by a thinner seasonal stratification. The next winter is then likely to connect again the new mixed layer with the upper core, while possibly keeping the primitive deeper core untouched. Such kind of interaction from one winter to another was observed in the Ierapetra eddy and is presented in Fig.10 (with same color code as in Fig.4a-f

and 5a-f). The Ierapetra eddy is a recurrent long-lived and intense anticyclone formed South-East of Crete (Theocharis et al.,
1993; Lascaratos and Tsantilas; Ioannou et al., 2017) and recently surveyed by the PERLE 1 and 2 campaigns (Ioannou et al.,
2019; Durrieu de Madron and Conan, 2019). Similarly to Eratosthenes anticyclones previously shown, the density anomaly is
mostly driven by a warm core, allowing to use temperature profile as a proxy for stratification (Ioannou et al., 2017). Figure 10
shows the Ierapetra anticyclone formed in autumn 2016. The first winter 2016-2017 turned out to be a 'non-connecting' event
('IER1' in Table1). Indeed in March 2017 a preexisting subsurface homogenized layer remains between 350 and 450m, below
the maximal anticyclonic core MLD of 220m (Fig.10c) and with about $+2$ °C temperature anomaly. From April to Decem-
ber 2017, summer heating restratified the upper layer and let below a second homogeneous layer between ~ 100 and 200m
deep. The primitive core remained homogenized at depth and separated by a temperature gradient throughout the summer
(Fig.10b). In January 2018 (Fig.10d), inside-eddy vertical profile shows the mixed layer deepening at 120m - already deeper
than the background MLD - and the double-core structure is still retrieved.At last at the end of February 2018 (Fig.10e), the
MLD completely eroded the seasonal stratification and connects the current MLD with previous winter subsurface core, then
reaching about 280m. The winter 2017-2018 is then a 'connecting' event ('IER2' in Table1). The timeseries is interrupted
inside the anticyclone, but Argo floats are again colocalized in May 2018, and despite some variability a temperature gradient
continuously separates the two cores between 200 and 250m (see Fig.10b). IER2 was then a 'connecting' event on a double-
core structure. The primitive anticyclonic core was not mixed but remained homogenized at depth. These data bring to light
a possible formation process of a double-core anticyclone through winter convection, and also documents for the first time the
fate of the formed subsurface anomaly, which can be tracked up to the next winter when it was mixed again.

5.3 Physical drivers

The observed importance of restratification delay $\Delta\tau$ should also have underlying physical mechanisms. Prolonged MLD
deepening and cooling inside-eddy (see examples in Fig.9) leads to the extreme MLD anomalies sometimes larger than 300m,
and hence marked MLD gradient occurring at the scale of the eddy radius or shorter. Indeed Gaube et al. (2019) found anoma-
lies on the order the mesoscale but in a composite vision and for large eddies compared to the deformation radius, MLD
gradients in eddies should occur on shorter scales (Meunier et al., 2018). Such marked MLD gradients should trigger mixed
layer instabilities leading to restratification (Boccaletti et al., 2007; Fox-Kemper et al., 2008), which calls for mechanisms
sustaining the mixing inside-eddy during the restratification delay. It should be noted that a homogenized layer itself does not
proof an active mixing, but still reveal the absence of restratification. We also interestingly noticed that in several cases Argo
floats remained well in the anticyclone core during the MLD deepening phase, but often leave the eddy soon after, maybe a
signature for mixed layer instabilities impacting the eddy. The first mechanism explaining longer mixing in anticyclones would
be an eddy modulation of air-sea fluxes by eddy-induced SSTA. Villas Bôas et al. (2015) observed such eddy-modulation on
air-sea sensible and latent heat fluxes, but in regions of energetic surface-intensified eddies, with very warm anticyclones (in
particular the Algulhas current retroflexion). For subsurface anticyclone, the eddy-induced SSTA is on the opposite expected
to be weakened (see the example of the cold-core anticyclone shown in Fig.4e and the study of Assassi et al. (2016)), and this

mechanism might then not be the most important. MLD deepening enhanced in anticyclones could be explained by other eddy retroactions than on the heat fluxes, a possible mechanism being the eddy-induced Ekman pumping (Stern, 1965; Gaube et al., 2015) or enhanced mixing in anticyclones due to near-inertial waves trapping (Kunze, 1985).

5.4 Impact on eddy dynamics

Connecting events also raise interesting questions on the consequence of such mixing of deeper subsurface anticyclone core, in particular the role of inside-eddy convection on the eddy dynamics itself. Studies in the literature mostly focused on winter convection inside cyclone because of the preconditioning with isopycnals doming at their center (Legg et al., 1998; Legg and McWilliams, 2001). Such phenomenon should also applied for subsurface anticyclone due to the surface isopycnals doming and subsequent stratification weakening (Assassi et al., 2016). The coincidence of observed multiple 'connecting' winters in long-lived anticyclones like the Mersa-Matruh and Eratosthenes structures suggests a possible mechanism regenerating these structure, and maybe explaining the extremely marked cyclone-anticyclone lifetime asymmetry in the Levantine basin (Mkhinini et al., 2014; Barboni et al., 2021). Interestingly Brenner (1993) already proposed winter cooling as possible mechanism explaining the sustained lifetime of the anticyclone surveyed south of Cyprus. The other structure calling for comparison is the Lofoten eddy in the Sea of Norway, and the Rockwall Trough eddy offshore Ireland, two long-lived deep anticyclonic structures. Winter convection was observed inside the core of the Lofoten eddy, and once thought to help regenerating the structure (Ivanov and Korablev, 1995; Köhl, 2007; Bosse et al., 2019). Double core formation was also observed in the Lofoten eddy (Bosse et al., 2019). Recent numerical studies showed this regeneration was primarily driven by merging of smaller structures (Köhl, 2007; Trodahl et al., 2020), however de Marez et al. (2021) showed that winter time convection eased this merging process by deepening of the eddy core. Merging of eddies detached from the coast towards an offshore anticyclonic attractor being also observed in the Levantine basin (Barboni et al., 2021), this could provide another explanation to long-lived Mediterranean anticyclones. Cylone-anticyclone asymmetry might not have just one mechanism, as other arguments were already proposed. Anticyclones have indeed a larger radius and are more coherent.

5.5 Biological impacts inside anticyclones

'Connecting' winter mixed layer in the Eratosthenes anticyclone was already observed by Krom et al. (1992) with a biogeochemical focus in 1989 (there called 'Cyprus eddy'). They measured a February inside-anticyclone MLD of 450m (compared to 200m) at the eddy boundary, with later spring restratification in May. Their temperature profile clearly corresponds to a 'connecting' event, with even deeper MLD than in our study. Comparing also nitrates, phosphates and chlorophyll, they showed that chlorophyll production was about 30% more abundant at the eddy core while relatively similar to Levantine basin average at its edge. The main nitracline was consistently measured below the winter mixed layer also at the eddy core, then around 450m. While spring phytoplankton bloom occurred at the surface, they observed a mixed homogeneous layer remaining aphotic, between the euphotic zone (the upper 120m) and this deep main nitracline (called 'decomposition zone' in Krom et al. (1992)). They observed instead here from February 1989 to January 1990 an increase of both nitrates and phosphates. Consequently in

the eddy a second nitracline formed at the bottom of the euphotic layer, at approximately the same level than a summer deep chlorophyll maximum. Similarly in another Eratosthenes structure in July 2008, Moutin and Prieur (2012) also estimated the maximal mixed layer in the previous winter to have reached 396m and let only a stratified thermocline below, another clear description of a 'connecting' winter mixing. Moutin and Prieur (2012) also observed in the eddy a main nitracline at roughly 400m depth, and a second one around 100m together with a deep chlorophyll maximum. The 100-400m depth zone remained with low mineralization and high value of dissolved organic matter (DOC). From these observations, it seems that a 'connecting' deep MLD induces a strong nutrient input to the euphotic layer, but letting in summer an homogenized aphotic subsurface layer with high DOC export at depth.

None of the two studies mentioned above observed the case of a 'non-connecting' MLD frequently observed in our study and also in an Eratosthenes anticyclone (see Fig.5). However Moutin and Prieur (2012) discussed this possibility : the winter MLD does not reach the main nitracline/phosphacline, it would keeps the upper layer away from the deep nutriment source. The whole system would then evolve towards an ultra-oligotrophic system because of nutrients being very weakly injected to the euphotic layer. This is expected to be in particular the case when a primitive subsurface core does not connect to the surface for several winter, such as the example of the Ierapetra anticyclone in Fig.10. The high frequency of 'non-connecting' anticyclone MLD observed in our study then suggest that anticyclones in the Eastern Mediterranean sea are ultra-oligotrophic systems more frequently than previously thought. Temporal evolution of such 'non-connecting' events with biogeochemical instruments such as BGC-Argo would be interesting to follow this analysis.

6   Conclusions

In this paper we were able to analyze, thanks to a combination of satellite observations and numerous in-situ data, several time series that finely describe the evolution of the winter mixed layer in the core of Mediterranean anticyclones. We even succeeded in following, for the same long-lived anticyclone, the evolution of its MLD over two consecutive years. This allowed us to quantify extreme anomalies induced by mesoscale eddies in the mixed layer, which would have been smoothed in a standard composite analysis. Indeed, we observed that the winter mixed layer can go down to 380 m in the core of Levantine Basin anticyclones, while the surrounding background MLD does not go deeper than 80 m or 100m.

We also observed a time lag of several weeks, and sometimes up to two months, in the spring restratification between the core of these deep anticyclones and the background sea, revealing that MLD temporal evolution is not uniform. Indeed, when the later restratifies due to rising temperature of the atmosphere, the core of these mesoscale anticyclones which are warmer continues to deepen and to cool. This time lag induces very strong spatial heterogeneities of the MLD in the eastern Mediterranean Sea during the early spring, with observed maximal MLD ranging from 50 to 330m.

We showed that this localized deepening of the MLD is controlled by the vertical structure of these eddies. When the surface mixing layer connects with the subsurface core of preexisting anticyclones, a rapid deepening of the surface mixed layer is observed. Conversely, when the surface mixed layer does not connect with the subsurface core, a double-core eddy is formed. Connection or not with preexisting subsurface core prove to be more relevant to describe MLD deepening than other eddy parameters such as SSH amplitude or size. MLD anomalies was observed to linearly increase with restratification delay, but increasing roughly 2 to 3 times faster for 'connecting' MLD than 'non-connecting' one.

These extreme MLD deepenings in anticyclone cores reveal complex and rich interaction between surface and subsurface of the eddies. Connection between the mixed layer and subsurface anomalies provide a way to propagate heat at depth while mixing in winter, which consequences that remain to be investigated. These winter deepening inside anticyclones could also play a role in sustaining the extremely long-lived anticyclone in the Eastern Mediterranean. MLD anomalies in cyclonic eddies remain to be investigated, and an open question would be to know if a restratification delay could also be observed in cyclones.

Data availability. CORA DT profiles (Szekely et al., 2019b) are freely available online on Copernicus marine service (CMEMS, https://marine.copernicus.eu/) under product name INSITU_GLO_TS_REP_OBSERVATIONS_013_001_b. Copernicus NRT profiles (Copernicus, 2021) are freely available on CMEMS under product name INSITU_GLO_NRT_OBSERVATIONS_013_030. DYNED Atlas eddy altimetric detections and contours from 2000 to 2019 is available at https://doi.org/10.14768/2019130201.2. AVISO SSHNRT day+6 1/8°data (Pujol, 2021) are freely available on CMEMS under product name SEALEVEL_EUR_PHY_L4_NRT_OBSERVATIONS_008_060 AMEDA eddy tracking algorithm is open source and available at https://github.com/briaclevu/AMEDA.

Author contributions. AB and SC built the methodology, performed the data analysis and investigation, wrote the manuscript and contributed equally to this work. AS supervised and validated the study and did funding acquisition. BL processed and produced eddy detections. FD provides in situ data in cooperation with SHOM cruises.

Competing interests. All authors declare they have no conflicts of interest.

Acknowledgements. The authors gratefully acknowledge the *Délégation Générale de l'Armement* which funded the program Protevs II into which the PERLE campaigns were scheduled, the French Naval Hydrologic and Oceanographic Service (SHOM) and the crew of the RV *L'Atalante* (Ifremer) for their contribution to the PERLE1 campaign, the crew of the RV *Pourquoi Pas ?* for their contribution to the PERLE2 campaign, and the one of the RV *Beautemps-Beaupré* for their contribution to the opportunity Arvor deployments in the Mersa-Matruh eddy in February 2021. The Argo data were collected and made freely available by the International Argo Program and the national programs that contribute to it (http://argo.jcommops.org/).

References

Amores, A., Jordà, G., and Monserrat, S.: Ocean eddies in the Mediterranean Sea from satellite altimetry: Sensitivity to satellite track location, Frontiers in Marine Science, p. 703, 2019.

Arai, M. and Yamagata, T.: Asymmetric evolution of eddies in rotating shallow water, Chaos: An Interdisciplinary Journal of Nonlinear Science, 4, 163–175, 1994.

Aroucha, L. C., Veleda, D., Lopes, F. S., Tyaquiçã, P., Lefèvre, N., and Araujo, M.: Intra- and Inter-Annual Variability of North Brazil Current Rings Using Angular Momentum Eddy Detection and Tracking Algorithm: Observations From 1993 to 2016, Journal of Geophysical Research: Oceans, 125, e2019JC015 921, https://doi.org/https://doi.org/10.1029/2019JC015921, https://agupubs.onlinelibrary.wiley.com/doi/abs/10.1029/2019JC015921, e2019JC015921 2019JC015921, 2020.

Assassi, C., Morel, Y., Vandermeirsch, F., Chaigneau, A., Pegliasco, C., Morrow, R., Colas, F., Fleury, S., Carton, X., Klein, P., et al.: An index to distinguish surface-and subsurface-intensified vortices from surface observations, Journal of Physical Oceanography, 46, 2529–2552, 2016.

Ayouche, A., De Marez, C., Morvan, M., L'hegaret, P., Carton, X., Le Vu, B., and Stegner, A.: Structure and dynamics of the Ras al Hadd oceanic dipole in the Arabian Sea, in: Oceans, vol. 2, pp. 105–125, MDPI, 2021.

Barboni, A., Lazar, A., Stegner, A., and Moschos, E.: Lagrangian eddy tracking reveals the Eratosthenes anticyclonic attractor in the eastern Levantine Basin, Ocean Science, 17, 1231–1250, 2021.

Belkin, I., Foppert, A., Rossby, T., Fontana, S., and Kincaid, C.: A Double-Thermostad Warm-Core Ring of the Gulf Stream, Journal of Physical Oceanography, 50, 489 – 507, https://doi.org/10.1175/JPO-D-18-0275.1, https://journals.ametsoc.org/view/journals/phoc/50/2/jpo-d-18-0275.1.xml, 2020.

Bevington, P. R., Robinson, D. K., Blair, J. M., Mallinckrodt, A. J., and McKay, S.: Data reduction and error analysis for the physical sciences, Computers in Physics, 7, 415–416, 1993.

Boccaletti, G., Ferrari, R., and Fox-Kemper, B.: Mixed layer instabilities and restratification, Journal of Physical Oceanography, 37, 2228–2250, 2007.

Bosse, A., Fer, I., Lilly, J. M., and Søiland, H.: Dynamical controls on the longevity of a non-linear vortex: The case of the Lofoten Basin Eddy, Scientific reports, 9, 1–13, 2019.

Brenner, S.: Long-term evolution and dynamics of a persistent warm core eddy in the Eastern Mediterranean Sea, Deep Sea Research Part II: Topical Studies in Oceanography, 40, 1193–1206, 1993.

Budillon, G., Gasparini, G., and Schroeder, K.: Persistence of an eddy signature in the central Tyrrhenian basin, Deep Sea Research Part II: Topical Studies in Oceanography, 56, 713–724, 2009.

Chelton, D. B., Schlax, M. G., and Samelson, R. M.: Global observations of nonlinear mesoscale eddies, Progress in oceanography, 91, 167–216, 2011.

Chen, Y., Speich, S., and Laxenaire, R.: Formation and Transport of the South Atlantic Subtropical Mode Water in Eddy-Permitting Observations, Journal of Geophysical Research: Oceans, 127, e2021JC017 767, 2022.

Copernicus: Copernicus Marine In Situ Tac Data Management Team : Global Ocean- In-Situ Near-Real-Time Observations, https://doi.org/10.48670/moi-00036, 2021.

D'Asaro, E. A.: The energy flux from the wind to near-inertial motions in the surface mixed layer, Journal of Physical Oceanography, 15, 1043–1059, 1985.

de Boyer Montégut, C., Madec, G., Fischer, A. S., Lazar, A., and Iudicone, D.: Mixed layer depth over the global ocean: An examination of profile data and a profile-based climatology, Journal of Geophysical Research: Oceans, 109, 2004.

620 de Marez, C., Le Corre, M., and Gula, J.: The influence of merger and convection on an anticyclonic eddy trapped in a bowl, Ocean Modelling, 167, 101 874, 2021.

Dong, S., Sprintall, J., Gille, S. T., and Talley, L.: Southern Ocean mixed-layer depth from Argo float profiles, Journal of Geophysical Research: Oceans, 113, 2008.

d'Ortenzio, F. and Ribera d'Alcà, M.: On the trophic regimes of the Mediterranean Sea: a satellite analysis, Biogeosciences, 6, 139–148, 625 2009.

d'Ortenzio, F., Iudicone, D., de Boyer Montégut, C., Testor, P., Antoine, D., Marullo, S., Santoleri, R., and Madec, G.: Seasonal variability of the mixed layer depth in the Mediterranean Sea as derived from in situ profiles, Geophysical Research Letters, 32, 2005.

d'Ortenzio, F., Taillandier, V., Claustre, H., Coppola, L., Conan, P., Dumas, F., Durrieu du Madron, X., Fourrier, M., Gogou, A., Karageorgis, A., et al.: BGC-Argo Floats Observe Nitrate Injection and Spring Phytoplankton Increase in the Surface Layer of Levantine Sea (Eastern 630 Mediterranean), Geophysical Research Letters, 48, e2020GL091 649, 2021.

Dufois, F., Hardman-Mountford, N. J., Greenwood, J., Richardson, A. J., Feng, M., and Matear, R. J.: Anticyclonic eddies are more productive than cyclonic eddies in subtropical gyres because of winter mixing, Science advances, 2, e1600 282, 2016.

Dugan, J., Mied, R., Mignerey, P., and Schuetz, A.: Compact, intrathermocline eddies in the Sargasso Sea, Journal of Geophysical Research: Oceans, 87, 385–393, 1982.

635 Durrieu de Madron, X. and Conan, P.: PERLE2 cruise, RV Pourquoi pas ?, https://doi.org/10.17600/18000865, 2019.

Fox-Kemper, B., Ferrari, R., and Hallberg, R.: Parameterization of mixed layer eddies. Part I: Theory and diagnosis, Journal of Physical Oceanography, 38, 1145–1165, 2008.

Frenger, I., Gruber, N., Knutti, R., and Münnich, M.: Imprint of Southern Ocean eddies on winds, clouds and rainfall, Nature geoscience, 6, 608–612, 2013.

640 Garreau, P., Dumas, F., Louazel, S., Stegner, A., and Le Vu, B.: High-Resolution Observations and Tracking of a Dual-Core Anticyclonic Eddy in the Algerian Basin, Journal of Geophysical Research: Oceans, 123, 9320–9339, 2018.

Gaube, P., Chelton, D. B., Samelson, R. M., Schlax, M. G., and O'Neill, L. W.: Satellite observations of mesoscale eddy-induced Ekman pumping, Journal of Physical Oceanography, 45, 104–132, 2015.

Gaube, P., J. McGillicuddy Jr, D., and Moulin, A. J.: Mesoscale eddies modulate mixed layer depth globally, Geophysical Research Letters, 645 46, 1505–1512, 2019.

Graves, L. P., McWilliams, J. C., and Montgomery, M. T.: Vortex evolution due to straining: A mechanism for dominance of strong, interior anticyclones, Geophysical and Astrophysical Fluid Dynamics, 100, 151–183, 2006.

Hamad, N., Millot, C., and Taupier-Letage, I.: The surface circulation in the eastern basin of the Mediterranean Sea, Scientia Marina, 70, 457–503, 2006.

650 Hausmann, U. and Czaja, A.: The observed signature of mesoscale eddies in sea surface temperature and the associated heat transport, Deep Sea Research Part I: Oceanographic Research Papers, 70, 60–72, 2012.

Hausmann, U., McGillicuddy Jr, D. J., and Marshall, J.: Observed mesoscale eddy signatures in Southern Ocean surface mixed-layer depth, Journal of Geophysical Research: Oceans, 122, 617–635, 2017.

Hayes, D., Zodiatis, G., Konnaris, G., Hannides, A., Solovyov, D., and Testor, P.: Glider transects in the Levantine Sea: Characteristics of the 655 warm core Cyprus eddy, in: OCEANS 2011 IEEE-Spain, pp. 1–9, IEEE, 2011.

He, Q., Zhan, H., Cai, S., He, Y., Huang, G., and Zhan, W.: A new assessment of mesoscale eddies in the South China Sea: Surface features, three-dimensional structures, and thermohaline transports, Journal of Geophysical Research: Oceans, 123, 4906–4929, 2018.

Holte, J. and Talley, L.: A new algorithm for finding mixed layer depths with applications to Argo data and Subantarctic Mode Water formation, Journal of Atmospheric and Oceanic Technology, 26, 1920–1939, 2009.

660 Holte, J., Talley, L. D., Gilson, J., and Roemmich, D.: An Argo mixed layer climatology and database, Geophysical Research Letters, 44, 5618–5626, 2017.

Houpert, L., Testor, P., De Madron, X. D., Somot, S., D'ortenzio, F., Estournel, C., and Lavigne, H.: Seasonal cycle of the mixed layer, the seasonal thermocline and the upper-ocean heat storage rate in the Mediterranean Sea derived from observations, Progress in Oceanography, 132, 333–352, 2015.

665 Ioannou, A., Stegner, A., Le Vu, B., Taupier-Letage, I., and Speich, S.: Dynamical evolution of intense Ierapetra eddies on a 22 year long period, Journal of Geophysical Research: Oceans, 122, 9276–9298, 2017.

Ioannou, A., Stegner, A., Tuel, A., LeVu, B., Dumas, F., and Speich, S.: Cyclostrophic corrections of AVISO/DUACS surface velocities and its application to mesoscale eddies in the Mediterranean Sea, Journal of Geophysical Research: Oceans, 124, 8913–8932, 2019.

Ioannou, A., Stegner, A., Dumas, F., and Le Vu, B.: Three-dimensional evolution of mesoscale anticyclones in the lee of Crete, Frontiers in
670   Marine Science, 7, 609 156, 2020.

Ivanov, V. and Korablev, A.: Formation and regeneration of intrapycnocline lense in the Norwegian Sea, Meteorologiya i Gidrologiya, pp. 102–110, 1995.

Köhl, A.: Generation and stability of a quasi-permanent vortex in the Lofoten Basin, Journal of Physical Oceanography, 37, 2637–2651, 2007.

675 Krom, M., Brenner, S., Kress, N., Neori, A., and Gordon, L.: Nutrient dynamics and new production in a warm-core eddy from the Eastern Mediterranean Sea, Deep Sea Research Part A. Oceanographic Research Papers, 39, 467–480, 1992.

Kunze, E.: Near-inertial wave propagation in geostrophic shear, Journal of Physical Oceanography, 15, 544–565, 1985.

Kurkin, A., Kurkina, O., Rybin, A., and Talipova, T.: Comparative analysis of the first baroclinic Rossby radius in the Baltic, Black, Okhotsk, and Mediterranean seas, Russian Journal of Earth Sciences, 20, 8, 2020.

680 Lacour, L., Briggs, N., Claustre, H., Ardyna, M., and Dall'Olmo, G.: The intraseasonal dynamics of the mixed layer pump in the subpolar North Atlantic Ocean: A Biogeochemical-Argo float approach, Global Biogeochemical Cycles, 33, 266–281, 2019.

Large, W. and Yeager, S.: On the observed trends and changes in global sea surface temperature and air–sea heat fluxes (1984–2006), Journal of Climate, 25, 6123–6135, 2012.

Lascaratos, A. and Tsantilas, S.: 1997. Study of the seasonal circle of the Ierapetra gyra, using satellite imager, in: Proc. Hell. Symp.
685   Oceanogr. Fish, vol. 1, pp. 165–168.

Lavigne, H., d'Ortenzio, F., Migon, C., Claustre, H., Testor, P., d'Alcalã, M. R., Lavezza, R., Houpert, L., and Prieur, L.: Enhancing the comprehension of mixed layer depth control on the Mediterranean phytoplankton phenology, Journal of Geophysical Research: Oceans, 118, 3416–3430, 2013.

Le Traon, P.-Y.: From satellite altimetry to Argo and operational oceanography: three revolutions in oceanography, Ocean Science, 9, 901–
690   915, 2013.

Le Vu, B., Stegner, A., and Arsouze, T.: Angular Momentum Eddy Detection and tracking Algorithm (AMEDA) and its application to coastal eddy formation, Journal of Atmospheric and Oceanic Technology, 35, 739–762, 2018.

Legg, S. and McWilliams, J. C.: Convective modifications of a geostrophic eddy field, Journal of physical oceanography, 31, 874–891, 2001.

Legg, S., McWilliams, J., and Gao, J.: Localization of deep ocean convection by a mesoscale eddy, Journal of Physical Oceanography, 28, 944–970, 1998.

Lévy, M., Ferrari, R., Franks, P. J., Martin, A. P., and Rivière, P.: Bringing physics to life at the submesoscale, Geophysical Research Letters, 39, 2012.

Lilly, J. M., Rhines, P. B., Schott, F., Lavender, K., Lazier, J., Send, U., and D'Asaro, E.: Observations of the Labrador Sea eddy field, Progress in Oceanography, 59, 75–176, 2003.

Liu, F., Zhou, H., Huang, W., and Wen, B.: Submesoscale Eddies Observation Using High-Frequency Radars: A Case Study in the Northern South China Sea, IEEE Journal of Oceanic Engineering, 46, 624–633, 2020.

L'Hévéder, B., Li, L., Sevault, F., and Somot, S.: Interannual variability of deep convection in the Northwestern Mediterranean simulated with a coupled AORCM, Climate dynamics, 41, 937–960, 2013.

McDougall, T., Feistel, R., Millero, F., Jackett, D., Wright, D., King, B., Marion, G., Chen, C., Spitzer, P., and Seitz, S.: The international thermodynamic equation of seawater 2010 (TEOS-10): Calculation and use of thermodynamic properties, Global ship-based repeat hydrography manual, IOCCP report no, 14, 2009.

Meunier, T., Pallás-Sanz, E., Tenreiro, M., Portela, E., Ochoa, J., Ruiz-Angulo, A., and Cusí, S.: The vertical structure of a Loop Current Eddy, Journal of Geophysical Research: Oceans, 123, 6070–6090, 2018.

Millot, C. and Taupier-Letage, I.: Circulation in the Mediterranean sea, The Mediterranean Sea, pp. 29–66, 2005.

Mkhinini, N., Coimbra, A. L. S., Stegner, A., Arsouze, T., Taupier-Letage, I., and Béranger, K.: Long-lived mesoscale eddies in the eastern Mediterranean Sea: Analysis of 20 years of AVISO geostrophic velocities, Journal of Geophysical Research: Oceans, 119, 8603–8626, 2014.

Moschos, E., Barboni, A., and Stegner, A.: Why do inverse eddy surface temperature anomalies emerge? The case of the Mediterranean Sea, submitted to JGR. Oceans, 2022.

Moutin, T. and Prieur, L.: Influence of anticyclonic eddies on the Biogeochemistry from the Oligotrophic to the Ultraoligotrophic Mediterranean (BOUM cruise), Biogeosciences, 9, 3827–3855, 2012.

Nilsson, C. and Cresswell, G.: The formation and evolution of East Australian Current warm-core eddies, Progress in oceanography, 9, 133–183, 1980.

Nof, D. and Dewar, W.: Alignment of lenses: Laboratory and numerical experiments, Deep Sea Research Part I: Oceanographic Research Papers, 41, 1207–1229, 1994.

Ozer, T., Gertman, I., Kress, N., Silverman, J., and Herut, B.: Interannual thermohaline (1979–2014) and nutrient (2002–2014) dynamics in the Levantine surface and intermediate water masses, SE Mediterranean Sea, Global and Planetary Change, 151, 60–67, 2017.

Parras-Berrocal, I. M., Vazquez, R., Cabos, W., Sein, D., Mañanes, R., Perez-Sanz, J., and Izquierdo, A.: The climate change signal in the Mediterranean Sea in a regionally coupled atmosphere–ocean model, Ocean Science, 16, 743–765, 2020.

Pegliasco, C., Delepoulle, A., Mason, E., Morrow, R., Faugère, Y., and Dibarboure, G.: META3. 1exp: a new global mesoscale eddy trajectory atlas derived from altimetry, Earth System Science Data, 14, 1087–1107, 2022.

Pettenuzzo, D., Large, W., and Pinardi, N.: On the corrections of ERA-40 surface flux products consistent with the Mediterranean heat and water budgets and the connection between basin surface total heat flux and NAO, Journal of Geophysical Research: Oceans, 115, 2010.

Poulain, P., Taupier-Letage, I., Gerin, R., Barbanti, R., Deponte, D., and Notarstefano, G.: Oceanographic Cruise EGITTO-1 R/V OGS–EXPLORA, 11–18 November 2005 Trieste, Italy to Port Said, Egypt, Cruise Report, Tech. rep., OGS Technical Report 29-2006-OGA-14, OGS, Trieste, Italy, 2006.

Pujol, M.-I.: Europeans Seas gridded L4 Sea Surface Height and derived variables NRT, https://doi.org/10.48670/moi-00142, 2021.

Smith, W. H. and Sandwell, D. T.: Global sea floor topography from satellite altimetry and ship depth soundings, Science, 277, 1956–1962, 1997.

735 Somot, S., Sevault, F., and Déqué, M.: Transient climate change scenario simulation of the Mediterranean Sea for the twenty-first century using a high-resolution ocean circulation model, Climate Dynamics, 27, 851–879, 2006.

Stegner, A., Le Vu, B., and Pegliasco, C.: Atlas of 3D Eddies in the Mediterranean Sea from 2000 to 2019, https://doi.org/10.14768/2019130201.2, 2019.

Stegner, A., Le Vu, B., Dumas, F., Ghannami, M. A., Nicolle, A., Durand, C., and Faugere, Y.: Cyclone-Anticyclone Asymmetry of Eddy
740 Detection on Gridded Altimetry Product in the Mediterranean Sea, Journal of Geophysical Research: Oceans, 126, e2021JC017 475, 2021.

Stern, M. E.: Interaction of a uniform wind stress with a geostrophic vortex, in: Deep Sea Research and Oceanographic Abstracts, vol. 12, pp. 355–367, Elsevier, 1965.

Szekely, T., Gourrion, J., Pouliquen, S., and Reverdin, G.: The CORA 5.2 dataset for global in situ temperature and salinity measurements: data description and validation, Ocean Science, 15, 1601–1614, https://doi.org/10.5194/os-15-1601-2019, https://os.copernicus.
745 org/articles/15/1601/2019/, 2019a.

Szekely, T., Gourrion, J., Pouliquen, S., Reverdin, G., and Merceur, F.: CORA, coriolis ocean dataset for reanalysis, https://doi.org/10.17882/46219, 2019b.

Taillandier, V., D'ortenzio, F., Prieur, L., Conan, P., Coppola, L., Cornec, M., Dumas, F., Durrieu de Madron, X., Fach, B., Fourrier, M., et al.: Sources of the Levantine Intermediate Water in winter 2019, Journal of Geophysical Research: Oceans, p. e2021JC017506, 2022.

750 Takahashi, T., Sutherland, S. C., Wanninkhof, R., Sweeney, C., Feely, R. A., Chipman, D. W., Hales, B., Friederich, G., Chavez, F., Sabine, C., et al.: Climatological mean and decadal change in surface ocean pCO2, and net sea–air CO2 flux over the global oceans, Deep Sea Research Part II: Topical Studies in Oceanography, 56, 554–577, 2009.

Theocharis, A., Georgopoulos, D., Lascaratos, A., and Nittis, K.: Water masses and circulation in the central region of the Eastern Mediterranean: Eastern Ionian, South Aegean and Northwest Levantine, 1986–1987, Deep sea research part II: topical studies in oceanography,
755 40, 1121–1142, 1993.

Trodahl, M., Isachsen, P. E., Lilly, J. M., Nilsson, J., and Kristensen, N. M.: The regeneration of the Lofoten Vortex through vertical alignment, Journal of Physical Oceanography, 50, 2689–2711, 2020.

Villas Bôas, A., Sato, O., Chaigneau, A., and Castelão, G.: The signature of mesoscale eddies on the air-sea turbulent heat fluxes in the South Atlantic Ocean, Geophysical Research Letters, 42, 1856–1862, 2015.

760 Williams, R. G.: Modification of ocean eddies by air-sea interaction, Journal of Geophysical Research: Oceans, 93, 15 523–15 533, 1988.
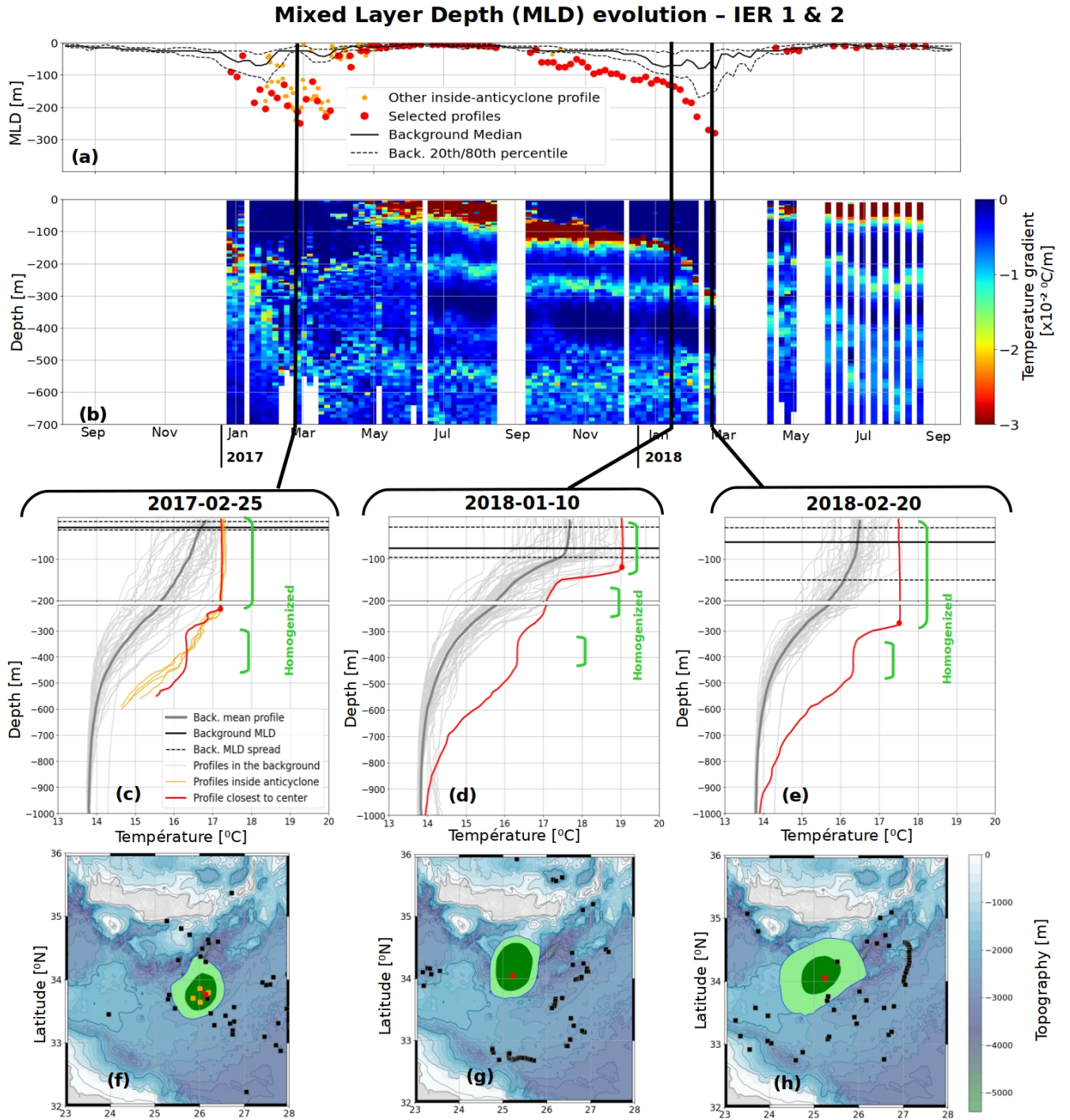
Figure 10. Same color codes and legend as in Fig.4 and 5, but for a Ierapetra anticyclone formed in 2016. Three vertical sections show respectively the mixing in early 2017 not reaching the deep subsurface core (panel c), the winter in early 2018 with a double-core, the shallow core from winter 2017-2018 and the deep core still untouched (panel d) and at last the MLD deepening in March 2018 connecting the anomaly formed in March 2017 with the surface (panel e).

Appendix A: In situ profile checking methodology

In both CORA-DT (Szekely et al., 2019b) and Copernicus-NRT (Copernicus, 2021) datasets vertical profiles data coming from XBT, CTD, glider and profiling floats are collected by selecting files with respective data type codes **XB, CT, GL, PF**. When a profile from 2000 to 2019 was available in both DT and NRT mode, it was retrieved from the CORA-DT dataset which
765 performs more quality checks (Szekely et al., 2019a). Selection was done with the following steps, separately for temperature and salinity, and when available, 'ADJUSTED' properties are collected :

- Position and date quality control (QC) flags equal to 1,2 or 5 and position not on land.

- First valid value (QC=1,2 or 5) above 50m, last valid value below 400m, and at least 40 measurements between 50 and 400m.

770 - Temperature data below 12°or above 35°are discarded, salinity data below 30 PSU or above 42 PSU are discarded. These parameters are specific to the Mediterranean sea.

- When both temperature and salinity are available, density is computed using the TEOS-10 equation (McDougall et al., 2009) from the Python package gsw (https://teos-10.github.io/GSW-Python/)

- Profiles are linearly interpolated on the same vertical grid, with 5m grid step from 5m to 300m depth and 10m grid step
775   from 300m to 2000m. Maximal gap allowed is 20m, and profiles with gaps are discarded.

- Profiles with temperature jumps higher than +6°C or -2°C (positive upwards) between two grid points are discarded, as assumed to be unrealistic. This is required in particular to filter out noisy XBT profiles.

- After these steps, only profiles with more than 40 data on the interpolated grid between 50 and 400m are kept.
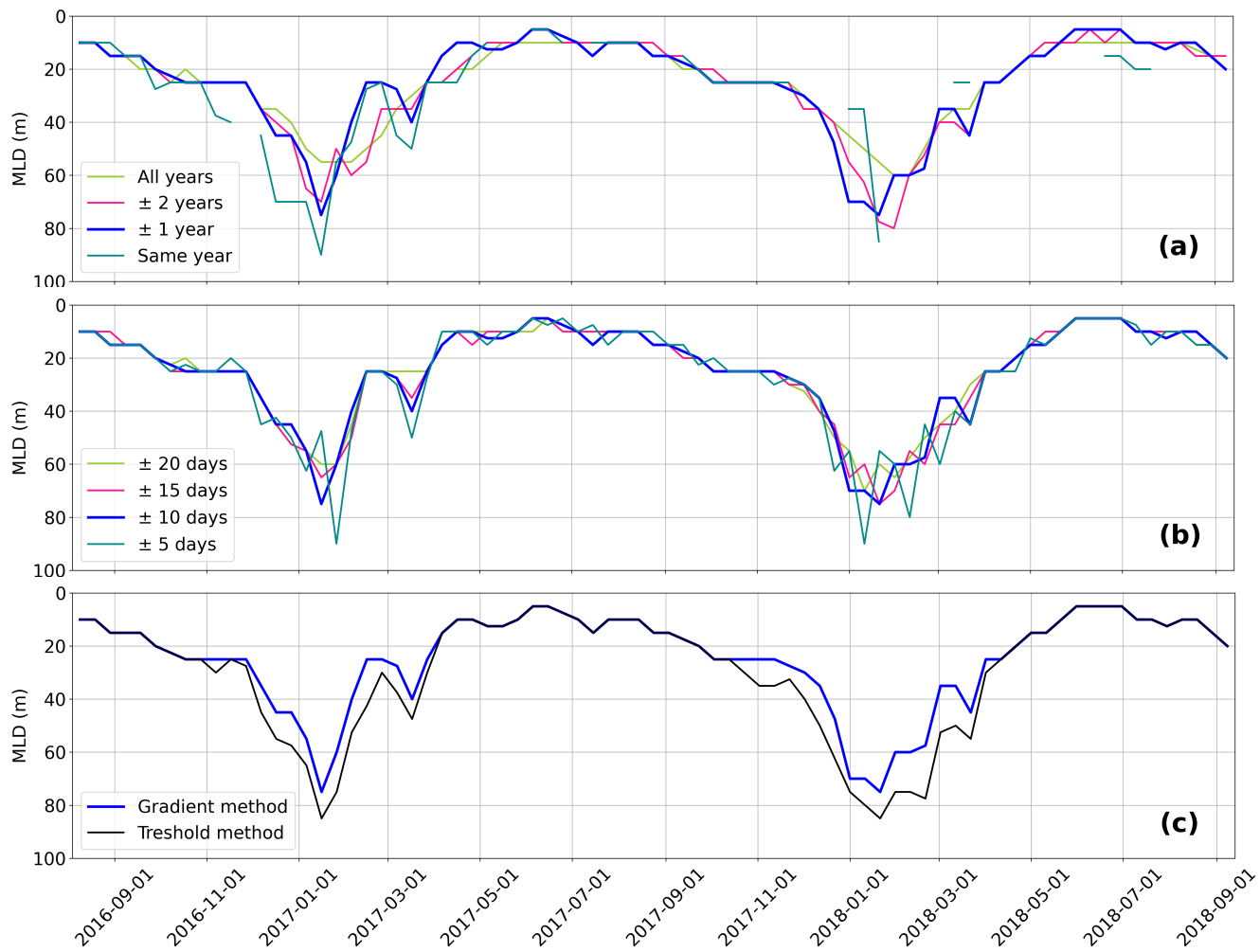
Figure A1. Sensitivity of the background MLD on the different parameters for events IER1-2 (see Table1 and Fig.10a) : (a) Δy (year interval) and (b) Δday (day interval). (c) Sensitivity to the MLD computation method. The background MLD method used throughout this study is $\Delta day = 10$ days, $\Delta y = 1$ year and the gradient method (common navy blue line on panels a-c).